

## University of Southampton Research Repository ePrints Soton

Copyright © and Moral Rights for this thesis are retained by the author and/or other copyright owners. A copy can be downloaded for personal non-commercial research or study, without prior permission or charge. This thesis cannot be reproduced or quoted extensively from without first obtaining permission in writing from the copyright holder/s. The content must not be changed in any way or sold commercially in any format or medium without the formal permission of the copyright holders.

When referring to this work, full bibliographic details including the author, title, awarding institution and date of the thesis must be given e.g.

AUTHOR (year of submission) "Full thesis title", University of Southampton, name of the University School or Department, PhD Thesis, pagination

# Correspondence

## 1 OFDMA/SC-FDMA-Aided Space–Time Shift Keying 2 for Dispersive Multiuser Scenarios

3 Mohammad Ismat Kadir, Shinya Sugiura, *Senior Member, IEEE*,  
4 Jiayi Zhang, Sheng Chen, *Fellow, IEEE*, and  
5 Lajos Hanzo, *Fellow, IEEE*

6 **Abstract**—Motivated by the recent concept of space–time shift keying  
7 (STSK), which was developed for achieving a flexible diversity versus  
8 multiplexing gain tradeoff, we propose a novel orthogonal frequency-  
9 division multiple access (OFDMA)/single-carrier frequency-division  
10 multiple-access (SC-FDMA)-aided multiuser STSK scheme for  
11 frequency-selective channels. The proposed OFDMA/SC-FDMA  
12 STSK scheme can provide an improved performance in dispersive  
13 channels while supporting multiple users in a multiple-antenna-aided  
14 wireless system. Furthermore, the scheme has the inherent potential of  
15 benefitting from the low-complexity single-stream maximum-likelihood  
16 detector. Both an uncoded and a sophisticated near-capacity-coded  
17 OFDMA/SC-FDMA STSK scheme were studied, and their performances  
18 were compared in multiuser wideband multiple-input–multiple-output  
19 (MIMO) scenarios. Explicitly, OFDMA/SC-FDMA-aided STSK exhibits  
20 an excellent performance, even in the presence of channel impairments  
21 due to the frequency selectivity of wideband channels, and proves to be a  
22 beneficial choice for high-capacity multiuser MIMO systems.

23 **Index Terms**—Author, please supply index terms/keywords  
24 for your paper. To download the IEEE Taxonomy go to  
25 [http://www.ieee.org/documents/2009Taxonomy\\_v101.pdf](http://www.ieee.org/documents/2009Taxonomy_v101.pdf).

## 26 I. INTRODUCTION

27 Recently the concept of space–time shift keying (STSK) [1], [2]  
28 has been developed to provide a highly flexible diversity versus  
29 multiplexing gain tradeoff at a low decoding complexity. Multiple-  
30 input–multiple-output (MIMO) systems can attain a beneficial mul-  
31 tiplexing gain by using, for example, BLAST or V-BLAST [3]. As  
32 a design alternative, they can also attain a diversity gain by using  
33 space–time block codes (STBCS) [4] or space–time trellis codes [5].  
34 As a further advance, linear dispersion codes were proposed [6], [7]  
35 to strike a flexible tradeoff between the achievable multiplexing and  
36 diversity gains, but at the cost of increased decoding complexity. As  
37 an additional design alternative, the concept of spatial modulation [8]  
38 emerged, which relies on using the transmit antenna index in addition  
39 to the conventional modulation constellation symbols to increase the  
40 attainable spectral efficiency. This scheme was then further developed  
41 to space shift keying (SSK) [9], which utilizes only the presence or

absence of the signal energy at a specific transmit antenna for data 42  
transmission. This SSK scheme imposes an extremely low decod- 43  
ing complexity. Motivated by these ideas, Sugiura *et al.* conceived 44  
a low-complexity STSK design, which outperformed the family of 45  
conventional MIMO arrangements. In particular, they proposed the 46  
activation of one out of  $Q$  dispersion matrices to appropriately spread 47  
the modulated symbols, thus facilitating a low-complexity single- 48  
stream maximum-likelihood (ML) detection based on the linearized 49  
MIMO model in [7]. 50

Although STSK-based systems have an excellent performance in 51  
narrowband channels, their performance in dispersive wireless chan- 52  
nels may erode. To mitigate the performance degradation imposed 53  
by dispersive channels, we intrinsically amalgamated the orthogo- 54  
nal frequency-division multiple-access (OFDMA) and single-carrier 55  
frequency-division multiple-access (SC-FDMA) concept with the 56  
STSK system. OFDMA/SC-FDMA-aided STSK systems can attain 57  
a superb diversity–multiplexing tradeoff, even in a multipath envi- 58  
ronment, while additionally supporting multiuser transmissions and 59  
maintaining a low peak-to-average-power ratio (PAPR) in uplink (UL) 60  
SC-FDMA/STSK scenarios. 61

Hence, OFDMA/SC-FDMA-assisted STSK systems are advocated 62  
in this paper, because OFDMA and SC-FDMA have been adopted for 63  
the downlink (DL) and the UL of the Long Term Evolution Advanced 64  
(LTE-Advanced) standard, respectively [10]. Before transmitting the 65  
signals from each of the transmit antenna elements (AEs) of our 66  
STSK system, either the discrete Fourier transform (DFT) or the 67  
original frequency-domain (FD) symbols are mapped to a number 68  
of subcarriers, either in a contiguous subband-based fashion or by 69  
dispersing them right across the entire FD. The resulting signal is 70  
then transmitted after the inverse discrete Fourier transform (IDFT) 71  
operation. 72

Thus, in this paper, a novel OFDMA/SC-FDMA-aided STSK 73  
MIMO architecture is proposed, which is capable of efficient 74  
operation in frequency-selective wireless channels to strike a 75  
flexible diversity versus multiplexing gain tradeoff. The transmit- 76  
ted signal of each subcarrier of the parallel modem experiences a 77  
nondispersive narrowband channel, and the overall STSK-based 78  
MIMO scheme exhibits a performance similar to that in narrow- 79  
band channels, despite operating in a wideband scenario. The ap- 80  
propriate mapping of the users' symbols to subcarriers results in 81  
a flexible multiuser performance while benefitting from our low- 82  
complexity single-stream based detection. We can use a single- 83  
tap MIMO FD equalizer based on the minimum mean square 84  
error or zero forcing, followed by single-stream-based detection 85  
in the TD. Furthermore, the DFT-precoding-based SC-FDMA 86  
scheme can reduce the PAPR for the mobile's UL transmissions. 87  
Finally, the performance of the proposed system that relies on 88  
a three-stage concatenated recursive systematic convolutional 89  
(RSC) and unity-rate-coding (URC) scenario is characterized 90  
through Extrinsic Information Transfer (EXIT) charts. 91

The remainder of this paper is organized as follows. In Section II, 92  
we present a brief overview of our proposed system, which re- 93  
lies on a linear dispersion-matrix-aided STSK scheme amalgamated 94  
with OFDMA/SC-FDMA transmission. In Section III, an OFDMA/ 95  
SC-FDMA STSK scheme based on a three-stage RSC-URC-coded 96  
scenario is discussed. Then, the performance of the scheme, 97

Manuscript received April 15, 2012; revised August 8, 2012; accepted  
September 16, 2012. This work was supported in part by the Research  
Councils U.K. (RC-UK) through the India–U.K. Advanced Technology Centre  
(IU-ATC), the China–U.K. Science Bridge, and the European Union (EU)  
through the Concerto Project. The review of this paper was coordinated  
by Dr. X. Wang.

M. Ismat Kadir, J. Zhang, S. Chen, and L. Hanzo are with the School  
of ECS, University of Southampton, SO17 1BJ Southampton, U.K. (e-mail:  
mik1g09@ecs.soton.ac.uk; sqc@ecs.soton.ac.uk; lh@ecs.soton.ac.uk).

S. Sugiura is with the Toyota Central R&D Laboratories Inc., Nagakute 480-  
1192, Japan (e-mail: sugiura@ieee.org).

Color versions of one or more of the figures in this paper are available online  
at <http://ieeexplore.ieee.org>.

Digital Object Identifier 10.1109/TVT.2012.2220794

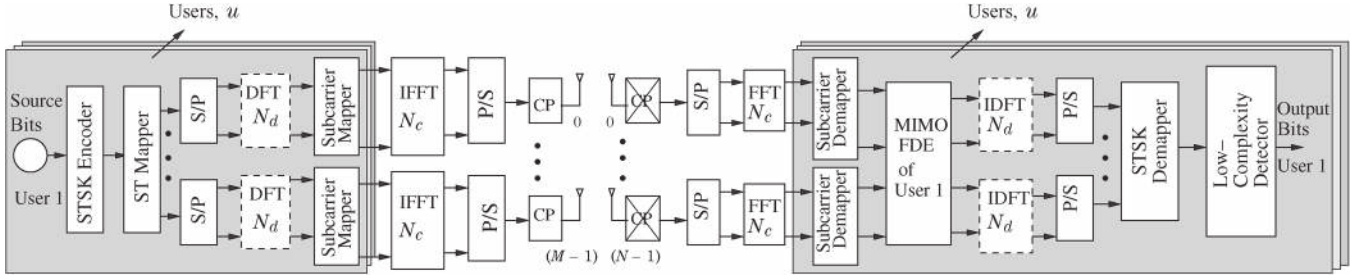


Fig. 1. Transmission model of the SC-FDMA-aided STSK scheme. In the OFDMA-aided scheme, the dotted blocks “DFT  $N_d$ ” in the transmitter and “IDFT  $N_d$ ” in the receiver do not exist. The STSK mapper selects one out of the  $Q$  dispersion matrices along with one constellation symbol, and the resulting space–time codewords are passed in different time slots through the OFDMA- or SC-FDMA-based multiuser transmission system before being transmitted through the transmit AEs. Because a single dispersion matrix is selected in one transmission block, a low-complexity single-stream ML detector can be employed.

98 particularly of an EXITnear-capacity design is investigated in  
99 Section IV. Finally, we conclude in Section V.

100 *Notations:* In general, we use boldface letters to denote matrices  
101 or column vectors, whereas  $\bullet^T$ ,  $\bullet^H$ ,  $\text{tr}(\bullet)$ , and  $\|\bullet\|$  represent the  
102 transpose, the Hermitian transpose, the trace, and the Euclidean norm  
103 of the matrix “ $\bullet$ ,” respectively. The notation  $\mathbf{a}[n_d]$  is used for the  
104  $n_d$ -th matrix of an array of matrices  $\mathbf{a}$ ,  $\mathbf{b}_{i,j}$  for the  $(i,j)$ -th entry  
105 of the matrix  $\mathbf{b}$ ; hence,  $\mathbf{a}_{i,j}[n_d]$  represents the  $(i,j)$ -th entry of the  
106  $n_d$ -th matrix of a matrix array  $\mathbf{a}$ . We use  $\text{vec}(\bullet)$  for the column-  
107 wise vectorial stacking operation to a matrix “ $\bullet$ ”  $\in \mathbb{C}^{C \times D}$  to yield  
108 a vector  $\in \mathbb{C}^{CD \times 1}$ ,  $\text{diag}\{a[0], a[1], \dots, a[N_c - 1]\}$  for a  $(N_c \times N_c)$   
109 diagonal matrix with  $a[0], a[1], \dots, a[N_c - 1]$  diagonal entries,  $\delta(\cdot)$   
110 for the Dirac delta function,  $\otimes$  for the Kronecker product and  $\circledast_{N_c}$   
111 for the  $(\text{length}-N_c)$  circular convolution operator. The notations  $\mathcal{F}_K$   
112 and  $\mathcal{F}_K^H$  denote the  $K$ -point DFT and IDFT matrices, respectively,  
113 and  $\mathbf{I}_K$  indicates the  $(K \times K)$ -element identity matrix. Furthermore,  
114 the generalized user is represented by  $u$ , whereas user  $u'$  refers to the  
115 desired user.

## 116 II. SYSTEM OVERVIEW

117 We consider an OFDMA/SC-FDMA STSK system with  $M$  transmit  
118 and  $N$  receive AEs. The channel is assumed to be a frequency-  
119 selective Rayleigh fading medium, which can be modeled by a finite  
120 impulse response filter with time-varying tap values [11], [12]. In our  
121 investigations of the system performance in Section IV, we have uti-  
122 lized the COST207-TU12 channel specifications for the delay and the  
123 Doppler power spectral density to represent a typical urban scenario.  
124 The number of subcarriers employed for the transmission of  $N_d$  STSK  
125 blocks of a single user after  $N_d$ -point DFT processing is  $N_c$ .

### 126 A. Transmitter

127 The transceiver architecture of our OFDMA/SC-FDMA STSK sys-  
128 tem is shown in Fig. 1. The signals are transmitted from different  
129 transmit AEs within  $T$  different symbol intervals after being mapped  
130 by the space–time (ST) mapper of the STSK block and after OFDMA/  
131 SC-FDMA-based processing. To be specific, the STSK encoder in  
132 Fig. 1 maps the source information of one of the  $U$  users to ST blocks  
133  $\mathbf{x}^u[n_d] \in \mathbb{C}^{M \times T}$ ,  $n_d = 0, 1, \dots, (N_d - 1)$  according to [2]

$$\mathbf{x}^u[n_d] = s^u[n_d] \mathbf{A}^u[n_d] \quad u = 0, 1, \dots, (U - 1) \quad (1)$$

134 where  $s^u[n_d]$  and  $\mathbf{A}^u[n_d]$  represent the  $u$ th user’s  $\mathcal{L}$ -phase-shift  
135 keying/quadratic-amplitude modulation (PSK/QAM) symbol and ac-  
136 tivated dispersion matrix (DM), respectively, from a set of  $Q$  such  
137 matrices  $\mathbf{A}_q$  ( $q = 1, 2, \dots, Q$ ), which are preassigned in advance  
138 of transmissions. The DMs may be generated, for example, either  
139 by maximizing the continuous-input–continuous-output memoryless

channel capacity or the discrete-input–continuous-output memory- 140  
less channel capacity or, alternatively, by minimizing the maximum 141  
pairwise symbol error probability (PSEP) under the power-constraint 142  
criterion [7], [13] of 143

$$\text{tr}(\mathbf{A}_q^H \mathbf{A}_q) = T \quad \forall q. \quad (2)$$

Thus, a block of  $\log_2(\mathcal{L} \cdot Q)$  number of bits are transmitted by the 144  
ST mapper in Fig. 1 per symbol interval, which forms an STSK ST 145  
block, and the STSK system in Fig. 1 is uniquely specified by the 146  
parameters  $(M, N, T, Q)$  in conjunction with the  $\mathcal{L}$ -PSK or  $\mathcal{L}$ -QAM 147  
scheme, where  $N$  is the number of receiver AEs. 148

After generating the ST blocks  $\mathbf{x}^u[n_d]$  for a particular user  $u$ , we 149  
employ frame-based transmission. In particular,  $N_c$  subcarriers are 150  
used for transmitting a frame, each frame consisting of  $N_d$  STSK 151  
blocks. To be specific, we define the transmit frame  $\tilde{\mathbf{x}}^u \in \mathbb{C}^{MN_d \times T}$  152  
for user  $u$  as 153

$$\tilde{\mathbf{x}}^u = \begin{bmatrix} \tilde{\mathbf{x}}_{0,0}^u & \tilde{\mathbf{x}}_{0,1}^u & \dots & \tilde{\mathbf{x}}_{0,(T-1)}^u \\ \tilde{\mathbf{x}}_{1,0}^u & \tilde{\mathbf{x}}_{1,1}^u & \dots & \tilde{\mathbf{x}}_{1,(T-1)}^u \\ \vdots & \vdots & \ddots & \vdots \\ \tilde{\mathbf{x}}_{(M-1),0}^u & \tilde{\mathbf{x}}_{(M-1),1}^u & \dots & \tilde{\mathbf{x}}_{(M-1),(T-1)}^u \end{bmatrix} \quad (3)$$

where each  $(N_d \times 1)$ -element data vector  $\tilde{\mathbf{x}}_{m,T_i}^u$ ,  $m = 0, 1, \dots, 154$   
 $(M - 1) T_i = 0, 1, \dots, (T - 1)$  can be represented by 155

$$\tilde{\mathbf{x}}_{m,T_i}^u = [\mathbf{x}_{m,T_i}^u[0], \mathbf{x}_{m,T_i}^u[1], \dots, \mathbf{x}_{m,T_i}^u[N_d - 1]]^T \quad (4)$$

which undergoes the  $N_d$ -point DFT operation. 156

To expound a little further, the data stream  $\tilde{\mathbf{x}}_{m,T_i}^u$  to be transmitted 157  
from the transmit AE  $m$  at a specific time interval  $T_i$  is first DFT 158  
preceded by the  $N_d$ -point DFT block; in case of OFDMA, however, 159  
this step is not required. Then, assuming a full-load system, the FD 160  
symbols  $\mathbf{X}_{m,T_i} \in \mathbb{C}^{N_d \times 1}$  output from the  $N_d$ -point DFT block of the 161  
SC-FDMA STSK scheme (or the direct FD STSK codeword symbols 162  
of the OFDMA STSK scheme) are mapped to  $N_c$  subcarriers with 163  
 $N_c = (N_d \times U)$ , where the subcarrier allocation may be in contiguous 164  
[localized frequency-division multiple-access (LFDMA)] [14] or an 165  
interleaved [interleaved frequency-division multiple-access (IFDMA)] 166  
[14] fashion. Denoting the set of subcarriers allocated to user  $u$  by  $\mathcal{S}_u$ , 167  
the subcarrier allocation matrix,  $\mathbf{P}^u \in \mathbb{C}^{N_c \times N_d}$  may be represented 168  
by [15] 169

$$\mathbf{P}_{n_c,n_d}^u = \begin{cases} 1, & \text{if } n_c \in \mathcal{S}_u \text{ and subcarrier } n_c \\ & \text{is allocated to } \mathcal{F}_{N_d} \mathbf{x}_{m,T_i}^u[n_d] \\ 0, & \text{otherwise} \end{cases} \quad (5)$$

where we have 170

$$n_c = \begin{cases} (n_d \times U) + u, & \text{IFDMA} \\ (N_d \times u) + n_d, & \text{LFDMA} \end{cases} \quad (6)$$

for all  $n_c = 0, 1, \dots, (N_c - 1)$  and all  $n_d = 0, 1, \dots, (N_d - 1)$ . 171

172 Defining  $\mathbf{C}_{add}(\bullet)$  as a matrix [16] that adds a TD cyclic prefix (CP)  
173 of length  $L_{cp}$  (which is higher than the channel's delay spread) to the  
174  $N_c$ -length vector  $(\bullet)$ , the TD data vector after the IDFT operation may  
175 be written as

$$\check{\mathbf{x}}_{m,T_i}^u = \mathbf{C}_{add} \left( \mathcal{F}_{N_c}^H \mathbf{P}^u \mathcal{F}_{N_d} \mathbf{x}_{m,T_i}^u \right) \quad (7)$$

$$= \mathbf{C}_{add} \left( \mathcal{F}_{N_c}^H \mathbf{P}^u \mathbf{X}_{m,T_i} \right). \quad (8)$$

176 Hence, the  $u$ th user's transmit frame after IDFT operation can be  
177 formulated in a similar form as (3), yielding

$$\check{\mathbf{x}}^u = \begin{bmatrix} \check{\mathbf{x}}_{0,0}^u & \check{\mathbf{x}}_{0,1}^u & \cdots & \check{\mathbf{x}}_{0,(T-1)}^u \\ \check{\mathbf{x}}_{1,0}^u & \check{\mathbf{x}}_{1,1}^u & \cdots & \check{\mathbf{x}}_{1,(T-1)}^u \\ \vdots & \vdots & \ddots & \vdots \\ \check{\mathbf{x}}_{(M-1),0}^u & \check{\mathbf{x}}_{(M-1),1}^u & \cdots & \check{\mathbf{x}}_{(M-1),(T-1)}^u \end{bmatrix} \quad (9)$$

178 where each vector  $\check{\mathbf{x}}_{m,T_i}^u$  is defined by (7) and (8) with

$$\check{\mathbf{x}}_{m,T_i}^u \in \mathbb{C}^{(N_c+L_{cp}) \times 1} \quad (10)$$

179 and hence

$$\check{\mathbf{x}}^u \in \mathbb{C}^{(N_c+L_{cp})M \times T}. \quad (11)$$

180 Each link of the  $M$  transmit and  $N$  receive AE-aided system is  
181 assumed to be frequency selective, whose channel impulse response  
182 (CIR) may be modeled as the ensemble of all the propagation paths  
183 [11], [12], i.e.,

$$h_{n,m}^u(t, \tau) = \sum_{l=0}^{(L-1)} a_l^u g_l^u(t) \delta(\tau - \tau_l^u) \quad (12)$$

184 for each  $n = 0, 1, \dots, (N-1)$ ,  $m = 0, 1, \dots, (M-1)$ , and  $u =$   
185  $0, 1, \dots, (U-1)$ . Here,  $L$  is the number of multipath components in  
186 the channel between the  $m$ th transmit and the  $n$ th receive AE, and  $a_l^u$ ,  
187  $\tau_l^u$ , and  $g_l^u(t)$  are the channel's envelope, delay, and Rayleigh fading  
188 process that exhibits a particular normalized Doppler frequency  $f_d$ ,  
189 respectively, associated with the  $l$ th path of user  $u$ .

190 Note that we use  $h$  and  $\mathbf{H}$  to denote the CIR and the  $(N \times$   
191  $M)$ -element CIR matrix, respectively, whereas  $\tilde{h}$  and  $\tilde{\mathbf{H}}$  denote  
192 the channel's frequency-domain channel transfer function (FDCHTF)  
193 and the  $(N \times M)$ -element frequency-domain channel transfer matrix  
194 (FDCHTM), respectively.

### 195 B. Receiver

196 Assuming perfect synchronization at the receiver in Fig. 1 and after  
197 removing the CP, the discrete-time input to the receiver's " $N_c$ -point  
198 IDFT" block at the receive AE  $n$  at time slot  $T_i$  is given by [17]

$$\mathbf{y}_{n,T_i} = \sum_{u=0}^{(U-1)} \sum_{m=0}^{(M-1)} \mathbf{h}_{n,m}^u \otimes_{N_c} \check{\mathbf{x}}_{m,T_i}^u + \mathbf{v}_{n,T_i} \quad (13)$$

199 where  $\otimes_{N_c}$  represents the length- $N_c$  circular convolution operator, and  
200  $\mathbf{v}_{n,T_i}$  is the noise vector.

201 Defining the FDCHTM by  $\tilde{\mathbf{H}}^u$ , the FD transmit codeword matrix  
202 after subcarrier mapping by  $\tilde{\mathbf{X}}^u$  and the FD additive white Gaussian  
203 noise (AWGN) matrix by  $\mathbf{V}$ , the FD output matrix  $\mathbf{Y}$  after the  $N_c$ -  
204 point DFT of our ST architecture may be written as

$$\mathbf{Y} = \sum_{u=0}^{(U-1)} \tilde{\mathbf{H}}^u \tilde{\mathbf{X}}^u + \mathbf{V} \quad (14)$$

205 where each  $(n, m)$ -th component of  $\tilde{\mathbf{H}}^u$  is formulated as

$$\tilde{\mathbf{H}}_{n,m}^u = \text{diag} \left\{ \tilde{h}_{n,m}^u[0], \tilde{h}_{n,m}^u[1], \dots, \tilde{h}_{n,m}^u[N_c - 1] \right\} \in \mathbb{C}^{N_c \times N_c} \quad (15)$$

where  $\tilde{h}_{n,m}^u$  denotes the FDCHTF that corresponds to user  $u$ , and the 206  
components of  $\tilde{\mathbf{X}}^u$ ,  $\mathbf{V}$ , and  $\mathbf{Y}$  are defined by 207

$$\tilde{\mathbf{X}}_{m,T_i}^u = \mathbf{P}^u \mathbf{X}_{m,T_i}^u \in \mathbb{C}^{N_c \times 1} \quad (16)$$

$$\mathbf{V}_{n,T_i} \in \mathbb{C}^{N_c \times 1} \quad (17)$$

$$\mathbf{Y}_{n,T_i} \in \mathbb{C}^{N_c \times 1}. \quad (18)$$

Hence, the components of  $\mathbf{Y}$  can be formulated based on (14) as 208

$$\mathbf{Y}_{n,T_i} = \sum_{u=0}^{U-1} \tilde{\mathbf{H}}_{n,m}^u \mathbf{P}^u \mathbf{X}_{m,T_i}^u + \mathbf{V}_{n,T_i} \quad (19)$$

$$= \sum_{u=0}^{U-1} \tilde{\mathbf{H}}_{n,m}^u \mathbf{P}^u \mathcal{F}_{N_d} \check{\mathbf{x}}_{m,T_i}^u + \mathbf{V}_{n,T_i}. \quad (20)$$

Now, after subcarrier demapping and MIMO frequency-domain 209  
equalization (FDE), the received symbols are passed through the " $N_d$ - 210  
point IDFT" block of user  $u'$ . Defining  $\tilde{\mathbf{P}}^u = [\mathbf{P}^u]^T$  as the subcarrier 211  
demapping matrix and  $\mathbf{W}^{u'}$  as the weight matrix of the MIMO ZF or 212  
MMSE FDE of user  $u'$ , which is given by [18] 213

$$\mathbf{W}^{u'} = \begin{cases} \left[ (\tilde{\mathbf{H}}^{u'})^H \tilde{\mathbf{H}}^{u'} \right]^{-1} (\tilde{\mathbf{H}}^{u'})^H & \text{ZF} \\ \left[ (\tilde{\mathbf{H}}^{u'})^H \tilde{\mathbf{H}}^{u'} + \sigma_N^2 \mathbf{I}_M \right]^{-1} (\tilde{\mathbf{H}}^{u'})^H & \text{MMSE} \end{cases} \quad (21)$$

where  $\sigma_N^2$  denotes the variance of the additive noise, the elements 214  
of the TD output  $\mathbf{z}^{u'}$  of user  $u'$  after the IDFT operation may be 215  
expressed as [15] 216

$$\mathbf{z}_{m,T_i}^{u'} = \mathcal{F}_{N_d}^H \tilde{\mathbf{P}}^{u'} \mathbf{W}^{u'} \times \left( \tilde{\mathbf{H}}_{n,m}^{u'} \mathbf{P}^{u'} \mathcal{F}_{N_d} \check{\mathbf{x}}_{m,T_i}^{u'} + \sum_{\substack{u=0 \\ u \neq u'}}^{U-1} \tilde{\mathbf{H}}_{n,m}^u \mathbf{P}^u \mathcal{F}_{N_d} \check{\mathbf{x}}_{m,T_i}^u \right) + \tilde{\mathbf{v}}_{m,T_i}^{u'} \quad (22)$$

where  $\mathbf{z}_{m,T_i}^{u'}$  and  $\mathbf{W}_{m,n}^{u'}$  are the  $(m, T_i)$ -th and  $(m, n)$ -th components 217  
of  $\mathbf{z}^{u'}$  and  $\mathbf{W}^{u'}$ , respectively. Because each  $\tilde{\mathbf{H}}_{n,m}^u$  is diagonal, we 218  
see based on (21) that each  $\mathbf{W}_{m,n}^{u'}$  will also be diagonal. Due to the 219  
diagonal nature of both  $\tilde{\mathbf{H}}_{n,m}^u$  and  $\mathbf{W}_{m,n}^{u'}$  and because 220

$$\tilde{\mathbf{P}}^u \mathbf{P}^u = \begin{cases} \mathbf{I}_{N_d}, & u = u' \\ 0, & u \neq u' \end{cases} \quad (23)$$

we have 221

$$\mathbf{z}_{m,T_i}^{u'} = \mathcal{F}_{N_d}^H \tilde{\mathbf{P}}^{u'} \mathbf{W}_{m,n}^{u'} \tilde{\mathbf{H}}_{n,m}^{u'} \mathbf{P}^{u'} \mathcal{F}_{N_d} \check{\mathbf{x}}_{m,T_i}^{u'} + \tilde{\mathbf{v}}_{m,T_i}^{u'}. \quad (24)$$

Based on (24), observe that, under the idealized assumption of 222  
perfect synchronization, perfect orthogonality of the users using dif- 223  
ferent subcarriers and by exploiting the perfectly diagonal nature 224  
of both  $\mathbf{W}_{m,n}^{u'}$  and of the FDCHTMs  $\tilde{\mathbf{H}}_{n,m}^{u'}$ , our scheme becomes 225  
free from multiuser interferences (MUIs). However, the symbols that 226  
are transmitted by a given user in the context of both the LFDMA 227  
and IFDMA schemes with MMSE equalization will experience some 228  
form of self-interference (SI) [15]. By contrast, the ZF scheme can 229  
completely mitigate the SI and the DFT matrices  $\mathcal{F}_{N_d}^H$  and  $\mathcal{F}_{N_d}$ , the 230  
subcarrier mapping and demapping matrices,  $\mathbf{P}^{u'}$  and  $\tilde{\mathbf{P}}^{u'}$ , and the 231  
FDCHTM  $\tilde{\mathbf{H}}^{u'}$ , and the MMSE equalization matrix  $\mathbf{W}^{u'}$  is absent in 232  
(24), although the scheme suffers from performance degradation due 233  
to the inherent noise enhancement process when a particular subcarrier 234

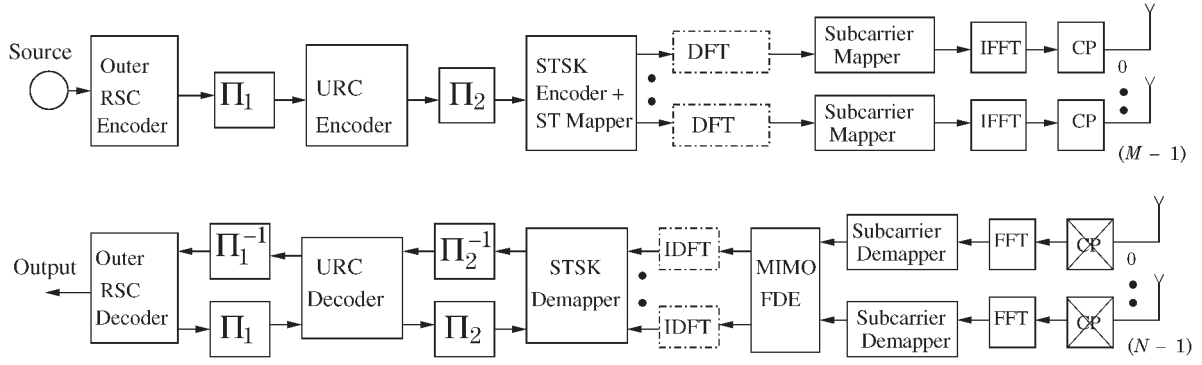


Fig. 2. Three-stage RSC-URC-coded OFDMA/SC-FDMA STSK transceiver. The dotted “DFT” block in the transmitter and the “IDFT” block in the receiver do not appear in the coded OFDMA STSK.

235 experiences deep fading. Hence, following the FD equalization and the  
236 receiver’s IDFT operation in Fig. 1, the decision variable  $z^{u'}$  for the  
237 ZF scheme can readily be written as

$$z^{u'}[n_d] = \tilde{x}^{u'}[n_d] + \tilde{v}^{u'}[n_d] \quad (25)$$

238 where  $\tilde{x}^{u'}[n_d] \in \mathbb{C}^{M \times T}$ , and  $\tilde{v}^{u'}[n_d] \in \mathbb{C}^{M \times T}$  for all  $n_d =$   
239  $0, 1, \dots, (N_d - 1)$ .

240 The IFDMA principle, on the other hand, increases the FD sepa-  
241 ration between the subcarriers and thereby provides some additional  
242 diversity gain. Thus, the decision variable of our scheme using ZF or  
243 assuming the mitigation of MMSE SI may be formulated, using the  
244 linearized system model in [7], as

$$\bar{z}^{u'}[n_d] = \chi \mathbf{k}^{u'} + \bar{v}^{u'}[n_d] \quad (26)$$

245 where  $\bar{z}^{u'}[n_d]$  is the  $(MT \times 1)$ -element matrix that was obtained by  
246 applying the vectorial stacking operation  $vec(\cdot)$  to the received FD sig-  
247 nal block  $z^{u'}[n_d]$ , whereas  $\chi = [vec(\mathbf{A}_1) \dots vec(\mathbf{A}_Q)] \in \mathbb{C}^{MT \times Q}$   
248 is the dispersion character matrix [13], and, finally,  $\bar{v}^{u'}[n_d] =$   
249  $vec(\tilde{v}^{u'}[n_d]) \in \mathbb{C}^{MT \times 1}$  is the stacked AWGN vector. Still referring  
250 to (26), the equivalent transmit signal vector is represented by

$$\mathbf{k}^{u'} = [0, \dots, 0, s^{u'}, 0, \dots, 0]^T \in \mathbb{C}^{Q \times 1} \quad (27)$$

251 where  $(q-1)$  and  $(Q-q)$  numbers of zeros surround the  $\mathcal{L}$ -PSK  
252 or  $\mathcal{L}$ -QAM symbol  $s^{u'}$  in the  $u'$ -th user’s equivalent transmit signal  
253 vector  $\mathbf{k}^{u'}$ , and the symbol  $s^{u'}$  is exactly located at the  $q$ th position,  
254 where  $q$  is the index of the activated DM.

255 We can now employ the single-stream-based ML detection [2] to  
256 detect the indices  $q$  and  $l_c$  of the DM activated and the constellation  
257 symbol used, respectively. The estimates  $(\hat{q}, \hat{l}_c)$  can be determined  
258 from

$$(\hat{q}, \hat{l}_c) = \arg \min_{q, l_c} \left\| \bar{z}^{u'}[n_d] - \chi \mathbf{k}_{q, l_c}^{u'} \right\|^2 \quad (28)$$

$$= \arg \min_{q, l_c} \left\| \bar{z}^{u'}[n_d] - (\chi)_q (s^{u'})_{l_c} \right\|^2 \quad (29)$$

259 where  $(s^{u'})_{l_c}$  is the  $l_c$ -th  $\mathcal{L}$ -PSK or the  $\mathcal{L}$ -QAM symbol,  $(\chi)_q$   
260 represents the  $q$ th column of  $\chi$ , and  $\mathbf{k}_{q, l_c}^{u'}$  is the equivalent transmit  
261 signal vector in (27) that corresponds to user  $u'$  at indices  $q$  and  $l_c$ .

262 In case of OFDMA, we have,  $\mathcal{F}_{N_d}^H = \mathcal{F}_{N_d} = \mathbf{I}_{N_d}$ . In other words,  
263 the blocks “ $N_d$ -point DFT” and “ $N_d$ -point IDFT” do not exist in  
264 OFDMA, and as such, the OFDMA scheme cannot benefit from  
265 the potential diversity provided by the DFT-based precoding stage.  
266 We can thus proceed with our ZF or MMSE weight matrix  $\mathbf{W}^{u'}$   
267 as aforementioned. Alternatively, for the OFDMA STSK, the ML

268 detector in [2] can directly be applied in the FD without employing  
269 the MIMO FDE. To be specific, in the absence of the weight matrix  
270  $\mathbf{W}^{u'}$  and with the substitution  $\mathcal{F}_{N_d}^H = \mathcal{F}_{N_d} = \mathbf{I}_{N_d}$ , (24) reduces to  
271  $\mathbf{Z}_{m, T_i}^{u'} = \tilde{\mathbf{H}}_{n, m}^{u'} \tilde{x}_{m, T_i}^{u'} + \tilde{v}_{m, T_i}^{u'}$ , where  $z_{m, T_i}^{u'}$  is replaced by  $\mathbf{Z}_{m, T_i}^{u'}$   
272 when the MIMO FDE is not employed. The direct ML detector in [2]  
273 for the OFDMA STSK scheme can thus be formulated as

$$(\hat{q}, \hat{l}_c) = \arg \min_{q, l_c} \left\| \bar{z}^{u'}[n_d] - \left( \bar{\mathbf{H}}^{u'}[n_d] \chi \right)_q (s^{u'})_{l_c} \right\|^2 \quad (30)$$

274 where  $\bar{z}^{u'}[n_d] = vec(\mathbf{Z}^{u'}[n_d])$ , and the equivalent FDCHTM  
275  $\bar{\mathbf{H}}^{u'}[n_d]$  is given by  $\bar{\mathbf{H}}^{u'}[n_d] = \mathbf{I}_T \otimes \tilde{\mathbf{H}}^{u'}[n_d]$ , whereas other no-  
276 tations are as used in (29).

277 In addition, we can see that our OFDMA/SC-FDMA STSK signal  
278 can be detected from (29) at a low complexity, because of the following  
279 two reasons.

- 1) Equation (29) does not explicitly contain either the FD channel  
280 transfer function or the TD CIR. Hence, data estimation using  
281 this equation involves a reduced number of multiplications and  
282 additions. 283
- 2) We can successfully employ the single-stream-based ML detec-  
284 tion that relies on the linearized model in [7], because only a  
285 single DM is activated at a given STSK block interval. 286

### III. CHANNEL-CODED OFDMA/SC-FDMA STSK 287

288 In this section, we investigate the three-stage parallel concatenated  
289 RSC-coded OFDMA/SC-FDMA STSK scheme in Fig. 2. The source  
290 bits are first convolutionally encoded and then interleaved by a random  
291 bit interleaver  $\Pi_1$ . A  $(2, 1, 2)$  RSC code is employed, and following  
292 channel interleaving, the symbols are precoded by a URC scheme,  
293 which was shown to be beneficial, because it efficiently spreads the  
294 extrinsic information as a benefit of its infinite impulse response [13].  
295 Then, the precoded bits are further interleaved by a second interleaver  
296  $\Pi_2$  in Fig. 2, and the interleaved bits are then transmitted by the  
297 OFDMA/SC-FDMA STSK scheme in the TD using an  $M$ -element  
298 MIMO transmitter.

299 As shown at the receiver in Fig. 2, after removing the CP, the  
300 received symbols are passed through the FFT unit, and the resulting  
301 FD symbols are then deallocated in an inverse fashion according to the  
302 IFDMA/LFDMA scheme used. The demapped symbols of a user are  
303 then equalized by the MIMO FDE, passed through another IDFT unit  
304 in Fig. 2 in accordance with the DFT precoding used, before they are  
305 then fed to the STSK demapper. We note that the equivalent received  
306 signal  $\bar{z}^{u'}$  carries  $B^{u'}$  channel-coded bits  $b^{u'} = [b_1^{u'}, b_2^{u'}, \dots, b_B^{u'}]$ ,

TABLE I  
 MAIN SIMULATION PARAMETERS

| Simulation parameter                | Value                    |
|-------------------------------------|--------------------------|
| Fast fading model                   | Corr. Rayleigh fading    |
| Normalized Doppler frequency, $f_d$ | 0.01                     |
| Channel specification               | COST207-TU12             |
| No. of subcarriers                  | 64                       |
| $N_d$ -point DFT precoder           | 16                       |
| Length of cyclic prefix             | 32                       |
| No. of Tx AE, $M$                   | 2                        |
| No. of Rx AE, $N$                   | 2                        |
| No. of Tx time slots, $T$           | 2                        |
| No. of dispersion matrices          | $Q = 2, 4$               |
| STSK specification                  | $(2, 2, 2, Q), Q = 2, 4$ |
| Modulation order                    | 2                        |
| Outer decoder                       | RSC (2, 1, 2)            |
| Generator polynomials               | $(g_r, g) = (3, 2)_8$    |
| Size of interleavers                | 4608000 bits             |
| Outer decoding iterations           | 9                        |
| Inner decoder                       | URC                      |
| Inner decoding iterations           | 2                        |

307 and the extrinsic log-likelihood ratio (LLR) of  $b_k^{u'}$ ,  $k = 1, \dots, B^{u'}$   
 308 can be expressed as [13]

$$L_e(b_k^{u'}) = \ln \frac{\sum_{\mathbf{k}_{q,l_c}^{u'}} \epsilon \mathbf{k}_1^{u'} e^{-\|\bar{\mathbf{z}}^{u'} - \chi \mathbf{k}_{q,l_c}^{u'}\|^2 / N_0 + \sum_{j \neq k} b_j^{u'} L_a(b_j^{u'})}}{\sum_{\mathbf{k}_{q,l_c}^{u'}} \epsilon \mathbf{k}_0^{u'} e^{-\|\bar{\mathbf{z}}^{u'} - \chi \mathbf{k}_{q,l_c}^{u'}\|^2 / N_0 + \sum_{j \neq k} b_j^{u'} L_a(b_j^{u'})}} \quad (31)$$

309 where  $L_a(\bullet)$  denotes the *a priori* LLR of the bits that correspond  
 310 to “•,” and  $\mathbf{k}_1^{u'}$  and  $\mathbf{k}_0^{u'}$  refer to the sets of the possible equivalent  
 311 transmit signal vectors  $\mathbf{k}^{u'}$  of user  $u'$  when  $b_k^{u'} = 1$  and  $b_k^{u'} = 0$ ,  
 312 respectively.

313 Then, the URC decoder in Fig. 2 processes the information provided  
 314 by the STSK demapper, in conjunction with the *a priori* information,  
 315 to generate the *a posteriori* probability. The URC generates extrinsic  
 316 information for both the RSC decoder and the demapper in Fig. 2.  
 317 The RSC channel decoder, which can be called the external decoder,  
 318 exchanges extrinsic information with the URC decoder and, after a  
 319 number of iterations, outputs the estimated bits. It is noteworthy here  
 320 that, for each of the outer iterations between the RSC decoder and the  
 321 URC, there are a number of inner iterations between the URC and the  
 322 STSK demapper.

#### 323 IV. PERFORMANCE OF THE PROPOSED SCHEME

324 We have investigated both the OFDMA-DL-and the SC-FDMA-  
 325 aided UL STSK schemes for both the IFDMA and LFDMA algorithms  
 326 using the simulation parameters in Table I.

327 Observe in Fig. 3 that the SC-FDMA STSK scheme that employs  
 328 MMSE equalization operating in an uncoded scenario exhibits better  
 329 bit-error rate (BER) performance than that of OFDMA STSK, which is  
 330 a benefit of the additional FD diversity attained by the DFT-precoding  
 331 in Fig. 1. The performance of IFDMA is shown to be better than the  
 332 LFDMA due to the higher FD separation between the subcarriers of  
 333 the same user, which hence results in independent FD fading. The  
 334 multiuser performance<sup>1</sup> attained is also investigated and is more or  
 335 less similar to the single-user scenario due to the absence of MUI  
 336 because of the diagonal nature of the weight matrix  $\mathbf{W}_{m,n}^{u'}$  in (24).  
 337 Furthermore, in Fig. 3, observe that SC-FDMA STSK exhibits better  
 338 performance than OFDMA STSK in both the LFDMA and IFDMA  
 339 regimes that employ MMSE-based FD equalization and ML detection.

<sup>1</sup>The multiuser performance curves for the uncoded scenario, however, are not included here for space economy.

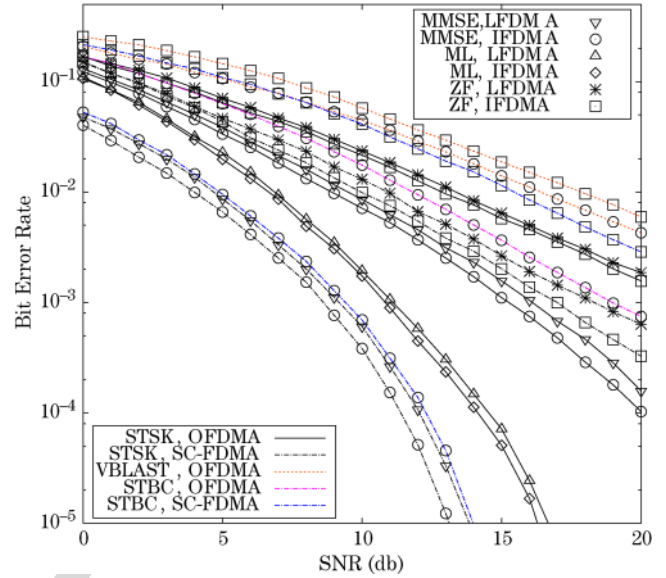


Fig. 3. Performance of the single-user OFDMA/SC-FDMA STSK (2, 2, 2, 2) system with BPSK modulation in a dispersive COST207-TU12 channel with different allocation schemes, ZF and MMSE FDE, and the ML detector in [2]. The performance of the scheme is also compared to V-BLAST ( $M, N$ ) = (2, 2), OFDMA, BPSK,  $\mathcal{G}_2$ -STBC ( $M, N$ ) = (2, 2), OFDMA/SC-FDMA, and BPSK benchmark under the same channel condition.

AQ5

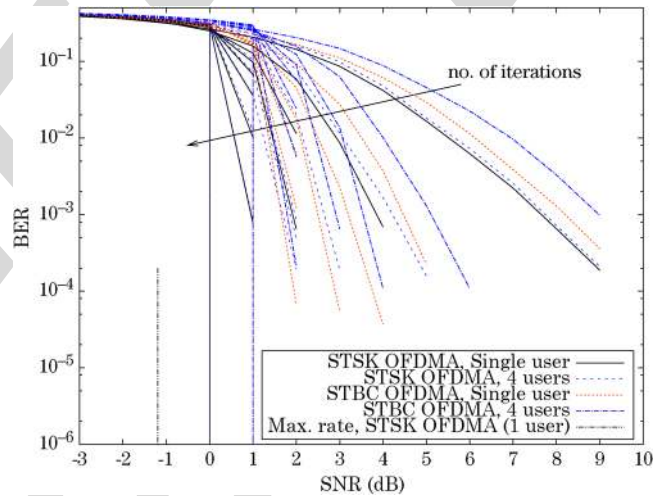


Fig. 4. BER performance of our channel-coded MMSE equalization-based OFDMA STSK (2, 2, 2, 2) that employs BPSK modulation in the dispersive COST207-TU12 channel and the corresponding  $\mathcal{G}_2$ -STBC scheme. The maximum achievable rate for the corresponding scheme for a single user, computed using the EXIT chart's area property, is also shown.

The achievable performance is, however, degraded, when ZF is used 340 due to the noise enhancement imposed. The performance of the pro- 341 posed STSK-based scheme is also compared to those of the V-BLAST- 342 aided [3] and  $\mathcal{G}_2$ -STBC-aided [4], [19] OFDMA/SC-FDMA schemes 343 using the same number of transmit and receive AEs ( $M, N$ ) and the 344 same throughput per block interval in Fig. 3, which demonstrates the 345 efficacy of the proposed scheme. 346

In Figs. 4 and 5, we also characterized the achievable BER perfor- 347 mance of the three-stage RSC- and URC-coded OFDMA/SC-FDMA 348 STSK (2, 2, 2, 2) binary phase-shift keying (BPSK) scheme that 349 relies on interleaved subcarrier allocation strategy in the context of 350 the wideband COST207-TU12 channel [11], where we employed 351 a half-rate RSC code with a constraint length of  $k_c = 2$  and the 352

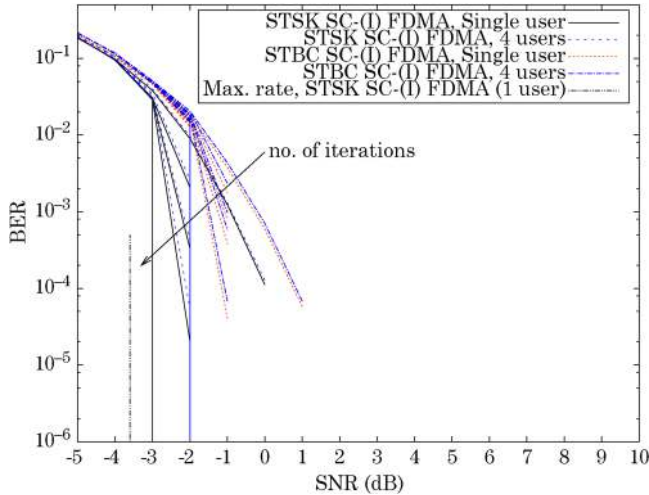


Fig. 5. Achievable BER performance of our channel-coded MMSE-based SC-FDMA STSK (2, 2, 2, 2) with BPSK modulation in the COST207-TU12 channel and the corresponding  $\mathcal{G}_2$ -STBC scheme with similar parameters. The maximum achievable rate of the corresponding scheme with a single user is also shown.

353 octally represented generator polynomials of  $(g_r, g) = (3, 2)_8$ , as  
 354 well as two random interleavers with a memory of 4 608 000 b. The  
 355 numbers of inner and outer decoder iterations were set to  $I_{inner} = 2$   
 356 and  $I_{outer} = 9$ , respectively. We also investigated the performance  
 357 of the SC-LFDMA scheme, and the performance was observed to  
 358 be similar to SC-IFDMA in the coded scenario. (However, the SC-  
 359 LFDMA performance figure has not been included here to limit the  
 360 total number of figures.) The performance of both the OFDMA STSK  
 361 and SC-(I)FDMA STSK has been compared to the corresponding  $\mathcal{G}_2$ -  
 362 STBC benchmarks. The maximum achievable rates of our schemes  
 363 were also calculated by exploiting the so-called area property of  
 364 EXIT charts. To be specific, it was shown in [20]–[22] that the area  
 365 under the inner decoder's EXIT curve at a certain signal-to-noise ratio  
 366 (SNR) quantifies the maximum achievable rate of the system, where an  
 367 infinitesimally low BER may be achieved. The SNRs that correspond  
 368 to the maximum achievable rates of the schemes are also shown in  
 369 Figs. 4 and 5.

370 Fig. 6 portrays the EXIT chart of the SC-FDMA STSK(2, 2, 2,  
 371 4) arrangement combined with QPSK modulation and the IFDMA  
 372 strategy, where the SNR was varied from  $-5$  dB to  $1$  dB in steps of  
 373  $0.5$  dB. It is shown that an open EXIT tunnel is formed at SNR =  
 374  $-4.0$  dB using an interleaver depth of 4 608 000 b. The corresponding  
 375 staircase-shaped decoding trajectory [22] based on bit-by-bit Monte  
 376 Carlo simulations conducted at  $-2.5$  dB is also shown. Thus, it can be  
 377 inferred that an infinitesimally low BER may be achieved at SNR =  
 378  $-2.5$  dB in a UL scenario after  $I_{outer} = 5$  iterations.

## V. CONCLUSION

380 In this paper, an OFDMA/SC-FDMA-aided STSK scheme has been  
 381 proposed, which overcomes the impairments of realistic dispersive  
 382 channels while facilitating multiuser transmissions. The scheme bene-  
 383 fits from the flexible diversity versus multiplexing gain tradeoff offered  
 384 by the recently developed STSK scheme that relies on low-complexity  
 385 single-stream-based ML detection. We quantified the relative merits of  
 386 OFDMA and SC-FDMA when combined with STSK and advocated  
 387 the SC-FDMA-based STSK scheme that relies on the interleaved  
 388 subcarrier allocation in the UL scenario as a benefit of its low PAPR.  
 389 The effects of the spatial correlation between the different AEs of a

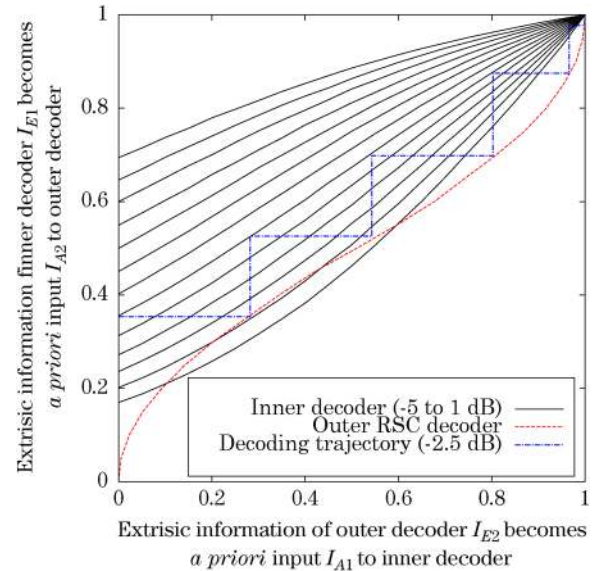


Fig. 6. EXIT trajectory of our three-stage turbo-detected MMSE-based SC-(I)FDMA STSK(2, 2, 2, 4) with QPSK modulation applied in a COST207-TU12 dispersive channel model with  $f_d = 0.01$ . The EXIT trajectory at  $-2.5$  dB is mapped on inner decoder EXIT curves from  $-5$  to  $1$  dB in steps of  $0.5$  dB and the outer RSC decoder EXIT function.

multiple antenna UL, however, have to further be investigated and will  
 be included in our future study.

It is worth mentioning here that the dispersion matrices invoked for  
 constructing our STSK system were optimized by an exhaustive search  
 to minimize the maximum PSEP under the power constraint in (2).  
 However, instead of using an exhaustive search method, a heuristic- or  
 genetic-algorithm-aided optimization of the dispersion matrices [23]–  
 [25] may also be investigated.

The EXIT charts of the proposed scheme converge to the (1.0, 1.0)  
 point of perfect convergence to a vanishingly low BER after a few  
 iterations, thus indicating a sharp decrease of the BER curve.

## REFERENCES

- [1] S. Sugiura, S. Chen, and L. Hanzo, "A universal space-time architec-  
 402 ture for multiple-antenna-aided systems," *IEEE Commun. Surveys Tuts.*, 403  
 vol. 14, no. 2, pp. 401–420, Jan. 2012. 404
- [2] S. Sugiura, S. Chen, and L. Hanzo, "Coherent and differential space-time  
 405 shift keying: A dispersion matrix approach," *IEEE Trans. Commun.*, 406  
 vol. 58, no. 11, pp. 3219–3230, Nov. 2010. 407
- [3] G. Foschini, G. Golden, R. Valenzuela, and P. Wolniansky, "Simplified  
 408 processing for high spectral efficiency wireless communication employ-  
 409 ing multielement arrays," *IEEE J. Sel. Areas Commun.*, vol. 17, no. 11, 410  
 pp. 1841–1852, Nov. 1999. 411
- [4] V. Tarokh, H. Jafarkhani, and A. Calderbank, "Space-time block codes  
 412 from orthogonal designs," *IEEE Trans. Inf. Theory*, vol. 45, no. 5, 413  
 pp. 1456–1467, Jul. 1999. 414
- [5] V. Tarokh, N. Seshadri, and A. Calderbank, "Space-time codes for  
 415 high-data-rate wireless communication: Performance criterion and code  
 416 construction," *IEEE Trans. Inf. Theory*, vol. 44, no. 2, pp. 744–765, 417  
 Mar. 1998. 418
- [6] B. Hassibi and B. M. Hochwald, "High-rate codes that are linear in  
 419 space and time," *IEEE Trans. Inf. Theory*, vol. 48, no. 7, pp. 1804–1824, 420  
 Jul. 2002. 421
- [7] R. W. Heath, Jr. and A. Paulraj, "Linear dispersion codes for MIMO  
 422 systems based on frame theory," *IEEE Trans. Signal Process.*, vol. 50, 423  
 no. 10, pp. 2429–2441, Oct. 2002. 424
- [8] R. Mesleh, H. Haas, S. Sinanovic, C. W. Ahn, and S. Yun, "Spatial  
 425 modulation," *IEEE Trans. Veh. Technol.*, vol. 57, no. 4, pp. 2228–2241, 426  
 Jul. 2008. 427
- [9] J. Jeganathan, A. Ghayeb, L. Szczecinski, and A. Ceron, "Space shift  
 428 keying modulation for MIMO channels," *IEEE Trans. Wireless Commun.*, 429  
 vol. 8, no. 7, pp. 3692–3703, Jul. 2009. 430

- 431 [10] A. Ghosh, R. Ratasuk, B. Mondal, N. Mangalvedhe, and T. Thomas,  
432 "LTE-Advanced: Next-generation wireless broadband technology," *IEEE*  
433 *Wireless Commun.*, vol. 17, no. 3, pp. 10–22, Jun. 2010.
- 434 [11] M. Patzold, *Mobile Fading Channels*. New York, NY: Wiley, 2003.
- 435 [12] R. Steele and L. Hanzo, *Mobile Radio Communications*, 2nd ed. New  
436 York, NY: Wiley, 1999.
- 437 [13] L. Hanzo, O. Alamri, M. El-Hajjar, and N. Wu, *Near-Capacity Multifunc-*  
438 *tional MIMO Systems (Sphere-Packing, Iterative Detection and Coopera-*  
439 *tion)*. New York: Wiley, May 2009.
- 440 [14] H. G. Myung, J. Lim, and D. J. Goodman, "Single-carrier FDMA for  
441 uplink wireless transmission," *IEEE Veh. Technol. Mag.*, vol. 1, no. 3,  
442 pp. 30–38, Sep. 2006.
- 443 [15] L. L. Yang, *Multicarrier Communications*. Chichester, U.K.: Wiley,  
444 Jan. 2009.
- 445 [16] A. Wilzeck, Q. Cai, M. Schiewer, and T. Kaiser, "Effect of multiple-carrier  
446 frequency offsets in MIMO SC-FDMA systems," in *Proc. Int. ITG/IEEE*  
447 *Workshop Smart Antennas*, Vienna, Austria, Feb. 2007.
- 448 [17] L. Hanzo, M. Munster, B. J. Choi, and T. Keller, *OFDM and MC-CDMA*  
449 *for Broadcasting Multiuser Communications, WLANs and Broadcasting*.  
450 New York: Wiley, Jul. 2003.
- 451 [18] J. R. Barry, E. A. Lee, and D. G. Messerschmitt, *Digital Communication*,  
452 3rd ed. Berlin, Germany: Springer-Verlag, 2003.
- [19] S. Alamouti, "A simple transmit diversity technique for wireless commu- 453  
nications," *IEEE J. Sel. Areas Commun.*, vol. 16, no. 8, pp. 1451–1458, 454  
Oct. 1998. 455
- [20] M. Tuchler, "Design of serially concatenated systems depending on the 456  
block length," *IEEE Trans. Commun.*, vol. 52, no. 2, pp. 209–218, 457  
Feb. 2004. 458
- [21] J. Hagenauer, "The EXIT chart—Introduction to extrinsic information 459  
transfer in iterative processing," in *Proc. Eur. Signal Process. Conf.*, 460  
Vienna, Austria, Sep. 2004, pp. 1541–1548. 461
- [22] S. Ten Brink, "Convergence behavior of iteratively decoded parallel con- 462  
catenated codes," *IEEE Trans. Commun.*, vol. 49, no. 10, pp. 1727–1737, 463  
Oct. 2001. 464
- [23] F. Babich, A. Crismani, M. Driusso, and L. Hanzo, "Design criteria 465  
and genetic algorithm aided optimization of three-stage concatenated 466  
space–time shift keying systems," *IEEE Signal Process. Lett.*, vol. 19, 467  
no. 8, pp. 543–546, Aug. 2012. 468
- [24] M. Jiang and L. Hanzo, "Unitary linear dispersion code design and opti- 469  
mization for MIMO communication systems," *IEEE Signal Process. Lett.*, 470  
vol. 17, no. 5, pp. 497–500, May 2010. 471
- [25] R. Rajashekar, K. Hari, and L. Hanzo, "Field-extension-code-based dis- 472  
persion matrices for coherently detected space–time shift keying," in 473  
*Proc. IEEE GLOBECOM*, Dec. 2011, pp. 1–5. 474

IEEE  
PROOF



## AUTHOR QUERIES

AUTHOR PLEASE ANSWER ALL QUERIES

AQ1 = Please provide keywords.

AQ2 = Acronyms that were mentioned only once should be spelled out, hence the omission of STTC, LDC, and SM. Please check if this is correct.

AQ3 = Editing was made to avoid confusion in hyphenations. Please check if this did not change the sentence's intended meaning.

AQ4 = Please check if the editing made did not change the sentence's intended meaning. Otherwise, provide the missing term or phrase.

AQ5 = Please check if the editing made (especially the use of serial comma) did not change the sentence's intended meaning. Otherwise, provide the missing term or phrase.

END OF ALL QUERIES

IEEE  
PROOF

# Correspondence

## 1 OFDMA/SC-FDMA-Aided Space–Time Shift Keying 2 for Dispersive Multiuser Scenarios

3 Mohammad Ismat Kadir, Shinya Sugiura, *Senior Member, IEEE*,  
4 Jiayi Zhang, Sheng Chen, *Fellow, IEEE*, and  
5 Lajos Hanzo, *Fellow, IEEE*

6 **Abstract**—Motivated by the recent concept of space–time shift keying  
7 (STSK), which was developed for achieving a flexible diversity versus  
8 multiplexing gain tradeoff, we propose a novel orthogonal frequency-  
9 division multiple access (OFDMA)/single-carrier frequency-division  
10 multiple-access (SC-FDMA)-aided multiuser STSK scheme for  
11 frequency-selective channels. The proposed OFDMA/SC-FDMA  
12 STSK scheme can provide an improved performance in dispersive  
13 channels while supporting multiple users in a multiple-antenna-aided  
14 wireless system. Furthermore, the scheme has the inherent potential of  
15 benefitting from the low-complexity single-stream maximum-likelihood  
16 detector. Both an uncoded and a sophisticated near-capacity-coded  
17 OFDMA/SC-FDMA STSK scheme were studied, and their performances  
18 were compared in multiuser wideband multiple-input–multiple-output  
19 (MIMO) scenarios. Explicitly, OFDMA/SC-FDMA-aided STSK exhibits  
20 an excellent performance, even in the presence of channel impairments  
21 due to the frequency selectivity of wideband channels, and proves to be a  
22 beneficial choice for high-capacity multiuser MIMO systems.

23 **Index Terms**—Author, please supply index terms/keywords  
24 for your paper. To download the IEEE Taxonomy go to  
25 [http://www.ieee.org/documents/2009Taxonomy\\_v101.pdf](http://www.ieee.org/documents/2009Taxonomy_v101.pdf).

## 26 I. INTRODUCTION

27 Recently the concept of space–time shift keying (STSK) [1], [2]  
28 has been developed to provide a highly flexible diversity versus  
29 multiplexing gain tradeoff at a low decoding complexity. Multiple-  
30 input–multiple-output (MIMO) systems can attain a beneficial mul-  
31 tiplexing gain by using, for example, BLAST or V-BLAST [3]. As  
32 a design alternative, they can also attain a diversity gain by using  
33 space–time block codes (STBCS) [4] or space–time trellis codes [5].  
34 As a further advance, linear dispersion codes were proposed [6], [7]  
35 to strike a flexible tradeoff between the achievable multiplexing and  
36 diversity gains, but at the cost of increased decoding complexity. As  
37 an additional design alternative, the concept of spatial modulation [8]  
38 emerged, which relies on using the transmit antenna index in addition  
39 to the conventional modulation constellation symbols to increase the  
40 attainable spectral efficiency. This scheme was then further developed  
41 to space shift keying (SSK) [9], which utilizes only the presence or

absence of the signal energy at a specific transmit antenna for data 42  
transmission. This SSK scheme imposes an extremely low decod- 43  
ing complexity. Motivated by these ideas, Sugiura *et al.* conceived 44  
a low-complexity STSK design, which outperformed the family of 45  
conventional MIMO arrangements. In particular, they proposed the 46  
activation of one out of  $Q$  dispersion matrices to appropriately spread 47  
the modulated symbols, thus facilitating a low-complexity single- 48  
stream maximum-likelihood (ML) detection based on the linearized 49  
MIMO model in [7]. 50

Although STSK-based systems have an excellent performance in 51  
narrowband channels, their performance in dispersive wireless chan- 52  
nels may erode. To mitigate the performance degradation imposed 53  
by dispersive channels, we intrinsically amalgamated the orthogo- 54  
nal frequency-division multiple-access (OFDMA) and single-carrier 55  
frequency-division multiple-access (SC-FDMA) concept with the 56  
STSK system. OFDMA/SC-FDMA-aided STSK systems can attain 57  
a superb diversity–multiplexing tradeoff, even in a multipath envi- 58  
ronment, while additionally supporting multiuser transmissions and 59  
maintaining a low peak-to-average-power ratio (PAPR) in uplink (UL) 60  
SC-FDMA/STSK scenarios. 61

Hence, OFDMA/SC-FDMA-assisted STSK systems are advocated 62  
in this paper, because OFDMA and SC-FDMA have been adopted for 63  
the downlink (DL) and the UL of the Long Term Evolution Advanced 64  
(LTE-Advanced) standard, respectively [10]. Before transmitting the 65  
signals from each of the transmit antenna elements (AEs) of our 66  
STSK system, either the discrete Fourier transform (DFT) or the 67  
original frequency-domain (FD) symbols are mapped to a number 68  
of subcarriers, either in a contiguous subband-based fashion or by 69  
dispersing them right across the entire FD. The resulting signal is 70  
then transmitted after the inverse discrete Fourier transform (IDFT) 71  
operation. 72

Thus, in this paper, a novel OFDMA/SC-FDMA-aided STSK 73  
MIMO architecture is proposed, which is capable of efficient 74  
operation in frequency-selective wireless channels to strike a 75  
flexible diversity versus multiplexing gain tradeoff. The transmit- 76  
ted signal of each subcarrier of the parallel modem experiences a 77  
nondispersive narrowband channel, and the overall STSK-based 78  
MIMO scheme exhibits a performance similar to that in narrow- 79  
band channels, despite operating in a wideband scenario. The ap- 80  
propriate mapping of the users' symbols to subcarriers results in 81  
a flexible multiuser performance while benefitting from our low- 82  
complexity single-stream based detection. We can use a single- 83  
tap MIMO FD equalizer based on the minimum mean square 84  
error or zero forcing, followed by single-stream-based detection 85  
in the TD. Furthermore, the DFT-precoding-based SC-FDMA 86  
scheme can reduce the PAPR for the mobile's UL transmissions. 87  
Finally, the performance of the proposed system that relies on 88  
a three-stage concatenated recursive systematic convolutional 89  
(RSC) and unity-rate-coding (URC) scenario is characterized 90  
through Extrinsic Information Transfer (EXIT) charts. 91

The remainder of this paper is organized as follows. In Section II, 92  
we present a brief overview of our proposed system, which re- 93  
lies on a linear dispersion-matrix-aided STSK scheme amalgamated 94  
with OFDMA/SC-FDMA transmission. In Section III, an OFDMA/ 95  
SC-FDMA STSK scheme based on a three-stage RSC-URC-coded 96  
scenario is discussed. Then, the performance of the scheme, 97

Manuscript received April 15, 2012; revised August 8, 2012; accepted  
September 16, 2012. This work was supported in part by the Research  
Councils U.K. (RC-UK) through the India–U.K. Advanced Technology Centre  
(IU-ATC), the China–U.K. Science Bridge, and the European Union (EU)  
through the Concerto Project. The review of this paper was coordinated  
by Dr. X. Wang.

M. Ismat Kadir, J. Zhang, S. Chen, and L. Hanzo are with the School  
of ECS, University of Southampton, SO17 1BJ Southampton, U.K. (e-mail:  
mik1g09@ecs.soton.ac.uk; sqc@ecs.soton.ac.uk; lh@ecs.soton.ac.uk).

S. Sugiura is with the Toyota Central R&D Laboratories Inc., Nagakute 480-  
1192, Japan (e-mail: sugiura@ieee.org).

Color versions of one or more of the figures in this paper are available online  
at <http://ieeexplore.ieee.org>.

Digital Object Identifier 10.1109/TVT.2012.2220794

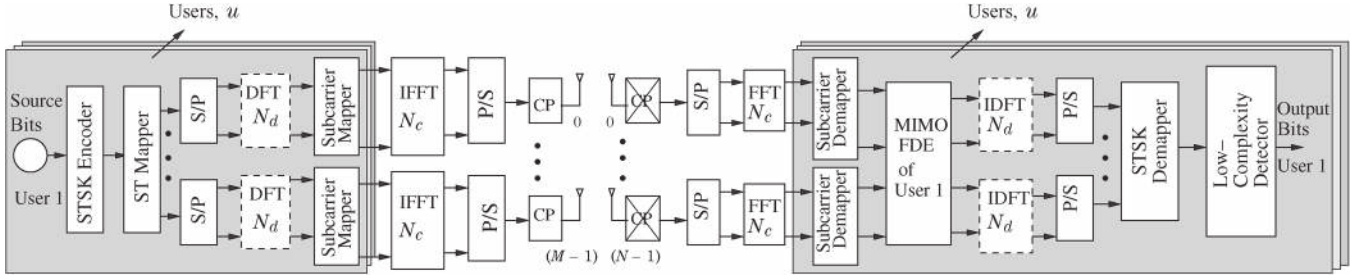


Fig. 1. Transmission model of the SC-FDMA-aided STSK scheme. In the OFDMA-aided scheme, the dotted blocks “DFT  $N_d$ ” in the transmitter and “IDFT  $N_d$ ” in the receiver do not exist. The STSK mapper selects one out of the  $Q$  dispersion matrices along with one constellation symbol, and the resulting space–time codewords are passed in different time slots through the OFDMA- or SC-FDMA-based multiuser transmission system before being transmitted through the transmit AEs. Because a single dispersion matrix is selected in one transmission block, a low-complexity single-stream ML detector can be employed.

98 particularly of an EXITnear-capacity design is investigated in  
99 Section IV. Finally, we conclude in Section V.

100 *Notations:* In general, we use boldface letters to denote matrices  
101 or column vectors, whereas  $\bullet^T$ ,  $\bullet^H$ ,  $\text{tr}(\bullet)$ , and  $\|\bullet\|$  represent the  
102 transpose, the Hermitian transpose, the trace, and the Euclidean norm  
103 of the matrix “ $\bullet$ ,” respectively. The notation  $\mathbf{a}[n_d]$  is used for the  
104  $n_d$ -th matrix of an array of matrices  $\mathbf{a}$ ,  $\mathbf{b}_{i,j}$  for the  $(i,j)$ -th entry  
105 of the matrix  $\mathbf{b}$ ; hence,  $\mathbf{a}_{i,j}[n_d]$  represents the  $(i,j)$ -th entry of the  
106  $n_d$ -th matrix of a matrix array  $\mathbf{a}$ . We use  $\text{vec}(\bullet)$  for the column-  
107 wise vectorial stacking operation to a matrix “ $\bullet$ ”  $\in \mathbb{C}^{C \times D}$  to yield  
108 a vector  $\in \mathbb{C}^{CD \times 1}$ ,  $\text{diag}\{a[0], a[1], \dots, a[N_c - 1]\}$  for a  $(N_c \times N_c)$   
109 diagonal matrix with  $a[0], a[1], \dots, a[N_c - 1]$  diagonal entries,  $\delta(\cdot)$   
110 for the Dirac delta function,  $\otimes$  for the Kronecker product and  $\circledast_{N_c}$   
111 for the  $(\text{length}-N_c)$  circular convolution operator. The notations  $\mathcal{F}_K$   
112 and  $\mathcal{F}_K^H$  denote the  $K$ -point DFT and IDFT matrices, respectively,  
113 and  $\mathbf{I}_K$  indicates the  $(K \times K)$ -element identity matrix. Furthermore,  
114 the generalized user is represented by  $u$ , whereas user  $u'$  refers to the  
115 desired user.

## 116 II. SYSTEM OVERVIEW

117 We consider an OFDMA/SC-FDMA STSK system with  $M$  transmit  
118 and  $N$  receive AEs. The channel is assumed to be a frequency-  
119 selective Rayleigh fading medium, which can be modeled by a finite  
120 impulse response filter with time-varying tap values [11], [12]. In our  
121 investigations of the system performance in Section IV, we have uti-  
122 lized the COST207-TU12 channel specifications for the delay and the  
123 Doppler power spectral density to represent a typical urban scenario.  
124 The number of subcarriers employed for the transmission of  $N_d$  STSK  
125 blocks of a single user after  $N_d$ -point DFT processing is  $N_c$ .

### 126 A. Transmitter

127 The transceiver architecture of our OFDMA/SC-FDMA STSK sys-  
128 tem is shown in Fig. 1. The signals are transmitted from different  
129 transmit AEs within  $T$  different symbol intervals after being mapped  
130 by the space–time (ST) mapper of the STSK block and after OFDMA/  
131 SC-FDMA-based processing. To be specific, the STSK encoder in  
132 Fig. 1 maps the source information of one of the  $U$  users to ST blocks  
133  $\mathbf{x}^u[n_d] \in \mathbb{C}^{M \times T}$ ,  $n_d = 0, 1, \dots, (N_d - 1)$  according to [2]

$$\mathbf{x}^u[n_d] = s^u[n_d] \mathbf{A}^u[n_d] \quad u = 0, 1, \dots, (U - 1) \quad (1)$$

134 where  $s^u[n_d]$  and  $\mathbf{A}^u[n_d]$  represent the  $u$ th user’s  $\mathcal{L}$ -phase-shift  
135 keying/quadratic-amplitude modulation (PSK/QAM) symbol and ac-  
136 tivated dispersion matrix (DM), respectively, from a set of  $Q$  such  
137 matrices  $\mathbf{A}_q$  ( $q = 1, 2, \dots, Q$ ), which are preassigned in advance  
138 of transmissions. The DMs may be generated, for example, either  
139 by maximizing the continuous-input–continuous-output memoryless

channel capacity or the discrete-input–continuous-output memory- 140  
less channel capacity or, alternatively, by minimizing the maximum 141  
pairwise symbol error probability (PSEP) under the power-constraint 142  
criterion [7], [13] of 143

$$\text{tr}(\mathbf{A}_q^H \mathbf{A}_q) = T \quad \forall q. \quad (2)$$

Thus, a block of  $\log_2(\mathcal{L} \cdot Q)$  number of bits are transmitted by the 144  
ST mapper in Fig. 1 per symbol interval, which forms an STSK ST 145  
block, and the STSK system in Fig. 1 is uniquely specified by the 146  
parameters  $(M, N, T, Q)$  in conjunction with the  $\mathcal{L}$ -PSK or  $\mathcal{L}$ -QAM 147  
scheme, where  $N$  is the number of receiver AEs. 148

After generating the ST blocks  $\mathbf{x}^u[n_d]$  for a particular user  $u$ , we 149  
employ frame-based transmission. In particular,  $N_c$  subcarriers are 150  
used for transmitting a frame, each frame consisting of  $N_d$  STSK 151  
blocks. To be specific, we define the transmit frame  $\tilde{\mathbf{x}}^u \in \mathbb{C}^{MN_d \times T}$  152  
for user  $u$  as 153

$$\tilde{\mathbf{x}}^u = \begin{bmatrix} \tilde{\mathbf{x}}_{0,0}^u & \tilde{\mathbf{x}}_{0,1}^u & \cdots & \tilde{\mathbf{x}}_{0,(T-1)}^u \\ \tilde{\mathbf{x}}_{1,0}^u & \tilde{\mathbf{x}}_{1,1}^u & \cdots & \tilde{\mathbf{x}}_{1,(T-1)}^u \\ \vdots & \vdots & \ddots & \vdots \\ \tilde{\mathbf{x}}_{(M-1),0}^u & \tilde{\mathbf{x}}_{(M-1),1}^u & \cdots & \tilde{\mathbf{x}}_{(M-1),(T-1)}^u \end{bmatrix} \quad (3)$$

where each  $(N_d \times 1)$ -element data vector  $\tilde{\mathbf{x}}_{m,T_i}^u$ ,  $m = 0, 1, \dots, 154$   
 $(M - 1) T_i = 0, 1, \dots, (T - 1)$  can be represented by 155

$$\tilde{\mathbf{x}}_{m,T_i}^u = [\mathbf{x}_{m,T_i}^u[0], \mathbf{x}_{m,T_i}^u[1], \dots, \mathbf{x}_{m,T_i}^u[N_d - 1]]^T \quad (4)$$

which undergoes the  $N_d$ -point DFT operation. 156

To expound a little further, the data stream  $\tilde{\mathbf{x}}_{m,T_i}^u$  to be transmitted 157  
from the transmit AE  $m$  at a specific time interval  $T_i$  is first DFT 158  
preceded by the  $N_d$ -point DFT block; in case of OFDMA, however, 159  
this step is not required. Then, assuming a full-load system, the FD 160  
symbols  $\mathbf{X}_{m,T_i} \in \mathbb{C}^{N_d \times 1}$  output from the  $N_d$ -point DFT block of the 161  
SC-FDMA STSK scheme (or the direct FD STSK codeword symbols 162  
of the OFDMA STSK scheme) are mapped to  $N_c$  subcarriers with 163  
 $N_c = (N_d \times U)$ , where the subcarrier allocation may be in contiguous 164  
[localized frequency-division multiple-access (LFDMA)] [14] or an 165  
interleaved [interleaved frequency-division multiple-access (IFDMA)] 166  
[14] fashion. Denoting the set of subcarriers allocated to user  $u$  by  $\mathcal{S}_u$ , 167  
the subcarrier allocation matrix,  $\mathbf{P}^u \in \mathbb{C}^{N_c \times N_d}$  may be represented 168  
by [15] 169

$$\mathbf{P}_{n_c,n_d}^u = \begin{cases} 1, & \text{if } n_c \in \mathcal{S}_u \text{ and subcarrier } n_c \\ & \text{is allocated to } \mathcal{F}_{N_d} \mathbf{x}_{m,T_i}^u[n_d] \\ 0, & \text{otherwise} \end{cases} \quad (5)$$

where we have 170

$$n_c = \begin{cases} (n_d \times U) + u, & \text{IFDMA} \\ (N_d \times u) + n_d, & \text{LFDMA} \end{cases} \quad (6)$$

for all  $n_c = 0, 1, \dots, (N_c - 1)$  and all  $n_d = 0, 1, \dots, (N_d - 1)$ . 171

172 Defining  $\mathbf{C}_{add}(\bullet)$  as a matrix [16] that adds a TD cyclic prefix (CP)  
173 of length  $L_{cp}$  (which is higher than the channel's delay spread) to the  
174  $N_c$ -length vector  $(\bullet)$ , the TD data vector after the IDFT operation may  
175 be written as

$$\check{\mathbf{x}}_{m,T_i}^u = \mathbf{C}_{add} \left( \mathcal{F}_{N_c}^H \mathbf{P}^u \mathcal{F}_{N_d} \mathbf{x}_{m,T_i}^u \right) \quad (7)$$

$$= \mathbf{C}_{add} \left( \mathcal{F}_{N_c}^H \mathbf{P}^u \mathbf{X}_{m,T_i} \right). \quad (8)$$

176 Hence, the  $u$ th user's transmit frame after IDFT operation can be  
177 formulated in a similar form as (3), yielding

$$\check{\mathbf{x}}^u = \begin{bmatrix} \check{\mathbf{x}}_{0,0}^u & \check{\mathbf{x}}_{0,1}^u & \cdots & \check{\mathbf{x}}_{0,(T-1)}^u \\ \check{\mathbf{x}}_{1,0}^u & \check{\mathbf{x}}_{1,1}^u & \cdots & \check{\mathbf{x}}_{1,(T-1)}^u \\ \vdots & \vdots & \ddots & \vdots \\ \check{\mathbf{x}}_{(M-1),0}^u & \check{\mathbf{x}}_{(M-1),1}^u & \cdots & \check{\mathbf{x}}_{(M-1),(T-1)}^u \end{bmatrix} \quad (9)$$

178 where each vector  $\check{\mathbf{x}}_{m,T_i}^u$  is defined by (7) and (8) with

$$\check{\mathbf{x}}_{m,T_i}^u \in \mathbb{C}^{(N_c+L_{cp}) \times 1} \quad (10)$$

179 and hence

$$\check{\mathbf{x}}^u \in \mathbb{C}^{(N_c+L_{cp})M \times T}. \quad (11)$$

180 Each link of the  $M$  transmit and  $N$  receive AE-aided system is  
181 assumed to be frequency selective, whose channel impulse response  
182 (CIR) may be modeled as the ensemble of all the propagation paths  
183 [11], [12], i.e.,

$$h_{n,m}^u(t, \tau) = \sum_{l=0}^{(L-1)} a_l^u g_l^u(t) \delta(\tau - \tau_l^u) \quad (12)$$

184 for each  $n = 0, 1, \dots, (N-1)$ ,  $m = 0, 1, \dots, (M-1)$ , and  $u =$   
185  $0, 1, \dots, (U-1)$ . Here,  $L$  is the number of multipath components in  
186 the channel between the  $m$ th transmit and the  $n$ th receive AE, and  $a_l^u$ ,  
187  $\tau_l^u$ , and  $g_l^u(t)$  are the channel's envelope, delay, and Rayleigh fading  
188 process that exhibits a particular normalized Doppler frequency  $f_d$ ,  
189 respectively, associated with the  $l$ th path of user  $u$ .

190 Note that we use  $h$  and  $\mathbf{H}$  to denote the CIR and the  $(N \times$   
191  $M)$ -element CIR matrix, respectively, whereas  $\tilde{h}$  and  $\tilde{\mathbf{H}}$  denote  
192 the channel's frequency-domain channel transfer function (FDCHTF)  
193 and the  $(N \times M)$ -element frequency-domain channel transfer matrix  
194 (FDCHTM), respectively.

### 195 B. Receiver

196 Assuming perfect synchronization at the receiver in Fig. 1 and after  
197 removing the CP, the discrete-time input to the receiver's " $N_c$ -point  
198 IDFT" block at the receive AE  $n$  at time slot  $T_i$  is given by [17]

$$\mathbf{y}_{n,T_i} = \sum_{u=0}^{(U-1)} \sum_{m=0}^{(M-1)} \mathbf{h}_{n,m}^u \otimes_{N_c} \check{\mathbf{x}}_{m,T_i}^u + \mathbf{v}_{n,T_i} \quad (13)$$

199 where  $\otimes_{N_c}$  represents the length- $N_c$  circular convolution operator, and  
200  $\mathbf{v}_{n,T_i}$  is the noise vector.

201 Defining the FDCHTM by  $\tilde{\mathbf{H}}^u$ , the FD transmit codeword matrix  
202 after subcarrier mapping by  $\tilde{\mathbf{X}}^u$  and the FD additive white Gaussian  
203 noise (AWGN) matrix by  $\mathbf{V}$ , the FD output matrix  $\mathbf{Y}$  after the  $N_c$ -  
204 point DFT of our ST architecture may be written as

$$\mathbf{Y} = \sum_{u=0}^{(U-1)} \tilde{\mathbf{H}}^u \tilde{\mathbf{X}}^u + \mathbf{V} \quad (14)$$

205 where each  $(n, m)$ -th component of  $\tilde{\mathbf{H}}^u$  is formulated as

$$\tilde{\mathbf{H}}_{n,m}^u = \text{diag} \left\{ \tilde{h}_{n,m}^u[0], \tilde{h}_{n,m}^u[1], \dots, \tilde{h}_{n,m}^u[N_c - 1] \right\} \in \mathbb{C}^{N_c \times N_c} \quad (15)$$

where  $\tilde{h}_{n,m}^u$  denotes the FDCHTF that corresponds to user  $u$ , and the 206  
components of  $\tilde{\mathbf{X}}^u$ ,  $\mathbf{V}$ , and  $\mathbf{Y}$  are defined by 207

$$\tilde{\mathbf{X}}_{m,T_i}^u = \mathbf{P}^u \mathbf{X}_{m,T_i}^u \in \mathbb{C}^{N_c \times 1} \quad (16)$$

$$\mathbf{V}_{n,T_i} \in \mathbb{C}^{N_c \times 1} \quad (17)$$

$$\mathbf{Y}_{n,T_i} \in \mathbb{C}^{N_c \times 1}. \quad (18)$$

Hence, the components of  $\mathbf{Y}$  can be formulated based on (14) as 208

$$\mathbf{Y}_{n,T_i} = \sum_{u=0}^{U-1} \tilde{\mathbf{H}}_{n,m}^u \mathbf{P}^u \mathbf{X}_{m,T_i}^u + \mathbf{V}_{n,T_i} \quad (19)$$

$$= \sum_{u=0}^{U-1} \tilde{\mathbf{H}}_{n,m}^u \mathbf{P}^u \mathcal{F}_{N_d} \check{\mathbf{x}}_{m,T_i}^u + \mathbf{V}_{n,T_i}. \quad (20)$$

Now, after subcarrier demapping and MIMO frequency-domain 209  
equalization (FDE), the received symbols are passed through the " $N_d$ - 210  
point IDFT" block of user  $u'$ . Defining  $\tilde{\mathbf{P}}^u = [\mathbf{P}^u]^T$  as the subcarrier 211  
demapping matrix and  $\mathbf{W}^{u'}$  as the weight matrix of the MIMO ZF or 212  
MMSE FDE of user  $u'$ , which is given by [18] 213

$$\mathbf{W}^{u'} = \begin{cases} \left[ (\tilde{\mathbf{H}}^{u'})^H \tilde{\mathbf{H}}^{u'} \right]^{-1} (\tilde{\mathbf{H}}^{u'})^H & \text{ZF} \\ \left[ (\tilde{\mathbf{H}}^{u'})^H \tilde{\mathbf{H}}^{u'} + \sigma_N^2 \mathbf{I}_M \right]^{-1} (\tilde{\mathbf{H}}^{u'})^H & \text{MMSE} \end{cases} \quad (21)$$

where  $\sigma_N^2$  denotes the variance of the additive noise, the elements 214  
of the TD output  $\mathbf{z}^{u'}$  of user  $u'$  after the IDFT operation may be 215  
expressed as [15] 216

$$\mathbf{z}_{m,T_i}^{u'} = \mathcal{F}_{N_d}^H \tilde{\mathbf{P}}^{u'} \mathbf{W}^{u'} \mathbf{y}_{m,n} \times \left( \tilde{\mathbf{H}}_{n,m}^{u'} \mathbf{P}^{u'} \mathcal{F}_{N_d} \check{\mathbf{x}}_{m,T_i}^{u'} + \sum_{\substack{u=0 \\ u \neq u'}}^{U-1} \tilde{\mathbf{H}}_{n,m}^u \mathbf{P}^u \mathcal{F}_{N_d} \check{\mathbf{x}}_{m,T_i}^u \right) + \tilde{\mathbf{v}}_{m,T_i}^{u'} \quad (22)$$

where  $\mathbf{z}_{m,T_i}^{u'}$  and  $\mathbf{W}_{m,n}^{u'}$  are the  $(m, T_i)$ -th and  $(m, n)$ -th components 217  
of  $\mathbf{z}^{u'}$  and  $\mathbf{W}^{u'}$ , respectively. Because each  $\tilde{\mathbf{H}}_{n,m}^u$  is diagonal, we 218  
see based on (21) that each  $\mathbf{W}_{m,n}^{u'}$  will also be diagonal. Due to the 219  
diagonal nature of both  $\tilde{\mathbf{H}}_{n,m}^u$  and  $\mathbf{W}_{m,n}^{u'}$  and because 220

$$\tilde{\mathbf{P}}^u \mathbf{P}^u = \begin{cases} \mathbf{I}_{N_d}, & u = u' \\ 0, & u \neq u' \end{cases} \quad (23)$$

we have 221

$$\mathbf{z}_{m,T_i}^{u'} = \mathcal{F}_{N_d}^H \tilde{\mathbf{P}}^{u'} \mathbf{W}_{m,n}^{u'} \tilde{\mathbf{H}}_{n,m}^{u'} \mathbf{P}^{u'} \mathcal{F}_{N_d} \check{\mathbf{x}}_{m,T_i}^{u'} + \tilde{\mathbf{v}}_{m,T_i}^{u'}. \quad (24)$$

Based on (24), observe that, under the idealized assumption of 222  
perfect synchronization, perfect orthogonality of the users using dif- 223  
ferent subcarriers and by exploiting the perfectly diagonal nature 224  
of both  $\mathbf{W}_{m,n}^{u'}$  and of the FDCHTMs  $\tilde{\mathbf{H}}_{n,m}^{u'}$ , our scheme becomes 225  
free from multiuser interferences (MUIs). However, the symbols that 226  
are transmitted by a given user in the context of both the LFDMA 227  
and IFDMA schemes with MMSE equalization will experience some 228  
form of self-interference (SI) [15]. By contrast, the ZF scheme can 229  
completely mitigate the SI and the DFT matrices  $\mathcal{F}_{N_d}^H$  and  $\mathcal{F}_{N_d}$ , the 230  
subcarrier mapping and demapping matrices,  $\mathbf{P}^{u'}$  and  $\tilde{\mathbf{P}}^{u'}$ , and the 231  
FDCHTM  $\tilde{\mathbf{H}}^{u'}$ , and the MMSE equalization matrix  $\mathbf{W}^{u'}$  is absent in 232  
(24), although the scheme suffers from performance degradation due 233  
to the inherent noise enhancement process when a particular subcarrier 234

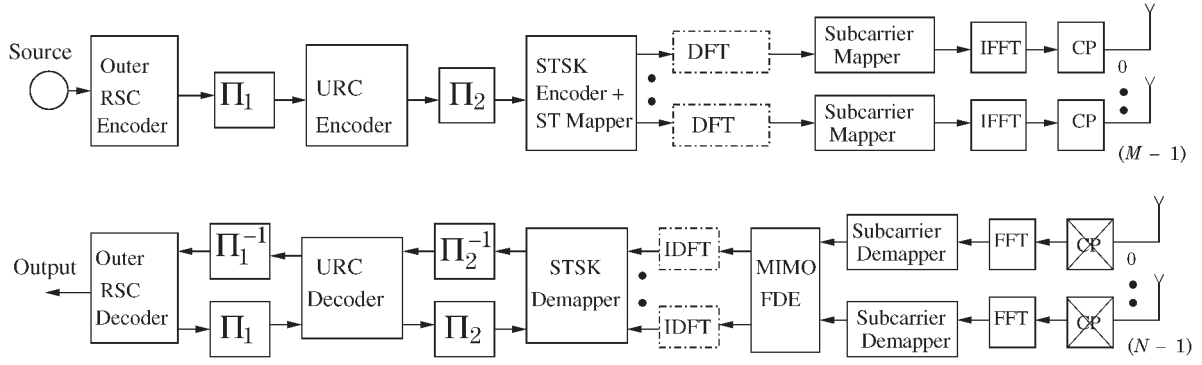


Fig. 2. Three-stage RSC-URC-coded OFDMA/SC-FDMA STSK transceiver. The dotted “DFT” block in the transmitter and the “IDFT” block in the receiver do not appear in the coded OFDMA STSK.

235 experiences deep fading. Hence, following the FD equalization and the  
236 receiver’s IDFT operation in Fig. 1, the decision variable  $z^{u'}$  for the  
237 ZF scheme can readily be written as

$$z^{u'}[n_d] = \tilde{x}^{u'}[n_d] + \tilde{v}^{u'}[n_d] \quad (25)$$

238 where  $\tilde{x}^{u'}[n_d] \in \mathbb{C}^{M \times T}$ , and  $\tilde{v}^{u'}[n_d] \in \mathbb{C}^{M \times T}$  for all  $n_d =$   
239  $0, 1, \dots, (N_d - 1)$ .

240 The IFDMA principle, on the other hand, increases the FD sepa-  
241 ration between the subcarriers and thereby provides some additional  
242 diversity gain. Thus, the decision variable of our scheme using ZF or  
243 assuming the mitigation of MMSE SI may be formulated, using the  
244 linearized system model in [7], as

$$\bar{z}^{u'}[n_d] = \chi \mathbf{k}^{u'} + \bar{v}^{u'}[n_d] \quad (26)$$

245 where  $\bar{z}^{u'}[n_d]$  is the  $(MT \times 1)$ -element matrix that was obtained by  
246 applying the vectorial stacking operation  $vec(\cdot)$  to the received FD sig-  
247 nal block  $z^{u'}[n_d]$ , whereas  $\chi = [vec(\mathbf{A}_1) \dots vec(\mathbf{A}_Q)] \in \mathbb{C}^{MT \times Q}$   
248 is the dispersion character matrix [13], and, finally,  $\bar{v}^{u'}[n_d] =$   
249  $vec(\tilde{v}^{u'}[n_d]) \in \mathbb{C}^{MT \times 1}$  is the stacked AWGN vector. Still referring  
250 to (26), the equivalent transmit signal vector is represented by

$$\mathbf{k}^{u'} = [0, \dots, 0, s^{u'}, 0, \dots, 0]^T \in \mathbb{C}^{Q \times 1} \quad (27)$$

251 where  $(q-1)$  and  $(Q-q)$  numbers of zeros surround the  $\mathcal{L}$ -PSK  
252 or  $\mathcal{L}$ -QAM symbol  $s^{u'}$  in the  $u'$ -th user’s equivalent transmit signal  
253 vector  $\mathbf{k}^{u'}$ , and the symbol  $s^{u'}$  is exactly located at the  $q$ th position,  
254 where  $q$  is the index of the activated DM.

255 We can now employ the single-stream-based ML detection [2] to  
256 detect the indices  $q$  and  $l_c$  of the DM activated and the constellation  
257 symbol used, respectively. The estimates  $(\hat{q}, \hat{l}_c)$  can be determined  
258 from

$$(\hat{q}, \hat{l}_c) = \arg \min_{q, l_c} \left\| \bar{z}^{u'}[n_d] - \chi \mathbf{k}_{q, l_c}^{u'} \right\|^2 \quad (28)$$

$$= \arg \min_{q, l_c} \left\| \bar{z}^{u'}[n_d] - (\chi)_q (s^{u'})_{l_c} \right\|^2 \quad (29)$$

259 where  $(s^{u'})_{l_c}$  is the  $l_c$ -th  $\mathcal{L}$ -PSK or the  $\mathcal{L}$ -QAM symbol,  $(\chi)_q$   
260 represents the  $q$ th column of  $\chi$ , and  $\mathbf{k}_{q, l_c}^{u'}$  is the equivalent transmit  
261 signal vector in (27) that corresponds to user  $u'$  at indices  $q$  and  $l_c$ .

262 In case of OFDMA, we have,  $\mathcal{F}_{N_d}^H = \mathcal{F}_{N_d} = \mathbf{I}_{N_d}$ . In other words,  
263 the blocks “ $N_d$ -point DFT” and “ $N_d$ -point IDFT” do not exist in  
264 OFDMA, and as such, the OFDMA scheme cannot benefit from  
265 the potential diversity provided by the DFT-based precoding stage.  
266 We can thus proceed with our ZF or MMSE weight matrix  $\mathbf{W}^{u'}$   
267 as aforementioned. Alternatively, for the OFDMA STSK, the ML

268 detector in [2] can directly be applied in the FD without employing  
269 the MIMO FDE. To be specific, in the absence of the weight matrix  
270  $\mathbf{W}^{u'}$  and with the substitution  $\mathcal{F}_{N_d}^H = \mathcal{F}_{N_d} = \mathbf{I}_{N_d}$ , (24) reduces to  
271  $\mathbf{Z}_{m, T_i}^{u'} = \tilde{\mathbf{H}}_{n, m}^{u'} \tilde{x}_{m, T_i}^{u'} + \tilde{v}_{m, T_i}^{u'}$ , where  $z_{m, T_i}^{u'}$  is replaced by  $\mathbf{Z}_{m, T_i}^{u'}$   
272 when the MIMO FDE is not employed. The direct ML detector in [2]  
273 for the OFDMA STSK scheme can thus be formulated as

$$(\hat{q}, \hat{l}_c) = \arg \min_{q, l_c} \left\| \bar{z}^{u'}[n_d] - \left( \bar{\mathbf{H}}^{u'}[n_d] \chi \right)_q (s^{u'})_{l_c} \right\|^2 \quad (30)$$

274 where  $\bar{z}^{u'}[n_d] = vec(\mathbf{Z}^{u'}[n_d])$ , and the equivalent FDCHTM  
275  $\bar{\mathbf{H}}^{u'}[n_d]$  is given by  $\bar{\mathbf{H}}^{u'}[n_d] = \mathbf{I}_T \otimes \tilde{\mathbf{H}}^{u'}[n_d]$ , whereas other no-  
276 tations are as used in (29).

277 In addition, we can see that our OFDMA/SC-FDMA STSK signal  
278 can be detected from (29) at a low complexity, because of the following  
279 two reasons.

- 1) Equation (29) does not explicitly contain either the FD channel  
280 transfer function or the TD CIR. Hence, data estimation using  
281 this equation involves a reduced number of multiplications and  
282 additions. 283
- 2) We can successfully employ the single-stream-based ML detec-  
284 tion that relies on the linearized model in [7], because only a  
285 single DM is activated at a given STSK block interval. 286

### III. CHANNEL-CODED OFDMA/SC-FDMA STSK 287

288 In this section, we investigate the three-stage parallel concatenated  
289 RSC-coded OFDMA/SC-FDMA STSK scheme in Fig. 2. The source  
290 bits are first convolutionally encoded and then interleaved by a random  
291 bit interleaver  $\Pi_1$ . A  $(2, 1, 2)$  RSC code is employed, and following  
292 channel interleaving, the symbols are precoded by a URC scheme,  
293 which was shown to be beneficial, because it efficiently spreads the  
294 extrinsic information as a benefit of its infinite impulse response [13].  
295 Then, the precoded bits are further interleaved by a second interleaver  
296  $\Pi_2$  in Fig. 2, and the interleaved bits are then transmitted by the  
297 OFDMA/SC-FDMA STSK scheme in the TD using an  $M$ -element  
298 MIMO transmitter.

299 As shown at the receiver in Fig. 2, after removing the CP, the  
300 received symbols are passed through the FFT unit, and the resulting  
301 FD symbols are then deallocated in an inverse fashion according to the  
302 IFDMA/LFDMA scheme used. The demapped symbols of a user are  
303 then equalized by the MIMO FDE, passed through another IDFT unit  
304 in Fig. 2 in accordance with the DFT precoding used, before they are  
305 then fed to the STSK demapper. We note that the equivalent received  
306 signal  $\bar{z}^{u'}$  carries  $B^{u'}$  channel-coded bits  $b^{u'} = [b_1^{u'}, b_2^{u'}, \dots, b_B^{u'}]$ ,

TABLE I  
 MAIN SIMULATION PARAMETERS

| Simulation parameter                | Value                    |
|-------------------------------------|--------------------------|
| Fast fading model                   | Corr. Rayleigh fading    |
| Normalized Doppler frequency, $f_d$ | 0.01                     |
| Channel specification               | COST207-TU12             |
| No. of subcarriers                  | 64                       |
| $N_d$ -point DFT precoder           | 16                       |
| Length of cyclic prefix             | 32                       |
| No. of Tx AE, $M$                   | 2                        |
| No. of Rx AE, $N$                   | 2                        |
| No. of Tx time slots, $T$           | 2                        |
| No. of dispersion matrices          | $Q = 2, 4$               |
| STSK specification                  | $(2, 2, 2, Q), Q = 2, 4$ |
| Modulation order                    | 2                        |
| Outer decoder                       | RSC (2, 1, 2)            |
| Generator polynomials               | $(g_r, g) = (3, 2)_8$    |
| Size of interleavers                | 4608000 bits             |
| Outer decoding iterations           | 9                        |
| Inner decoder                       | URC                      |
| Inner decoding iterations           | 2                        |

307 and the extrinsic log-likelihood ratio (LLR) of  $b_k^{u'}$ ,  $k = 1, \dots, B^{u'}$   
 308 can be expressed as [13]

$$L_e(b_k^{u'}) = \ln \frac{\sum_{\mathbf{k}_{q,l_c}^{u'}} \epsilon \mathbf{k}_1^{u'} e^{-\|\bar{\mathbf{z}}^{u'} - \chi \mathbf{k}_{q,l_c}^{u'}\|^2 / N_0 + \sum_{j \neq k} b_j^{u'} L_a(b_j^{u'})}}{\sum_{\mathbf{k}_{q,l_c}^{u'}} \epsilon \mathbf{k}_0^{u'} e^{-\|\bar{\mathbf{z}}^{u'} - \chi \mathbf{k}_{q,l_c}^{u'}\|^2 / N_0 + \sum_{j \neq k} b_j^{u'} L_a(b_j^{u'})}} \quad (31)$$

309 where  $L_a(\bullet)$  denotes the *a priori* LLR of the bits that correspond  
 310 to “•,” and  $\mathbf{k}_1^{u'}$  and  $\mathbf{k}_0^{u'}$  refer to the sets of the possible equivalent  
 311 transmit signal vectors  $\mathbf{k}^{u'}$  of user  $u'$  when  $b_k^{u'} = 1$  and  $b_k^{u'} = 0$ ,  
 312 respectively.

313 Then, the URC decoder in Fig. 2 processes the information provided  
 314 by the STSK demapper, in conjunction with the *a priori* information,  
 315 to generate the *a posteriori* probability. The URC generates extrinsic  
 316 information for both the RSC decoder and the demapper in Fig. 2.  
 317 The RSC channel decoder, which can be called the external decoder,  
 318 exchanges extrinsic information with the URC decoder and, after a  
 319 number of iterations, outputs the estimated bits. It is noteworthy here  
 320 that, for each of the outer iterations between the RSC decoder and the  
 321 URC, there are a number of inner iterations between the URC and the  
 322 STSK demapper.

#### 323 IV. PERFORMANCE OF THE PROPOSED SCHEME

324 We have investigated both the OFDMA-DL-and the SC-FDMA-  
 325 aided UL STSK schemes for both the IFDMA and LFDMA algorithms  
 326 using the simulation parameters in Table I.

327 Observe in Fig. 3 that the SC-FDMA STSK scheme that employs  
 328 MMSE equalization operating in an uncoded scenario exhibits better  
 329 bit-error rate (BER) performance than that of OFDMA STSK, which is  
 330 a benefit of the additional FD diversity attained by the DFT-precoding  
 331 in Fig. 1. The performance of IFDMA is shown to be better than the  
 332 LFDMA due to the higher FD separation between the subcarriers of  
 333 the same user, which hence results in independent FD fading. The  
 334 multiuser performance<sup>1</sup> attained is also investigated and is more or  
 335 less similar to the single-user scenario due to the absence of MUI  
 336 because of the diagonal nature of the weight matrix  $\mathbf{W}_{m,n}^{u'}$  in (24).  
 337 Furthermore, in Fig. 3, observe that SC-FDMA STSK exhibits better  
 338 performance than OFDMA STSK in both the LFDMA and IFDMA  
 339 regimes that employ MMSE-based FD equalization and ML detection.

<sup>1</sup>The multiuser performance curves for the uncoded scenario, however, are not included here for space economy.

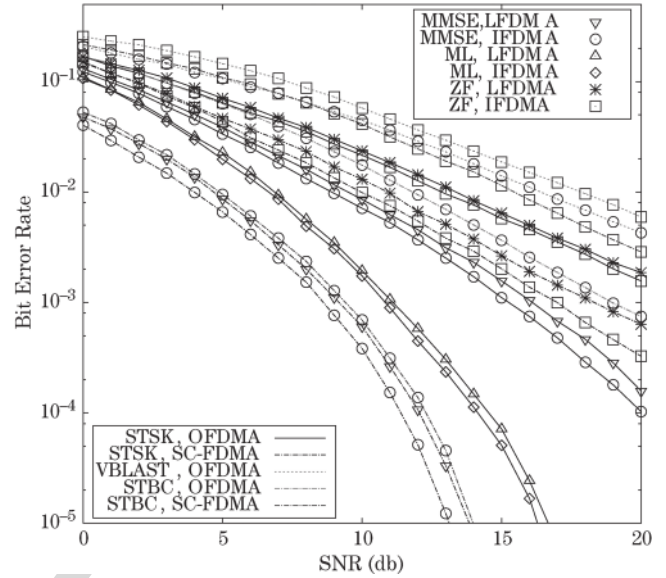


Fig. 3. Performance of the single-user OFDMA/SC-FDMA STSK (2, 2, 2, 2) system with BPSK modulation in a dispersive COST207-TU12 channel with different allocation schemes, ZF and MMSE FDE, and the ML detector in [2]. The performance of the scheme is also compared to V-BLAST ( $M, N$ ) = (2, 2), OFDMA, BPSK,  $\mathcal{G}_2$ -STBC ( $M, N$ ) = (2, 2), OFDMA/SC-FDMA, and BPSK benchmark under the same channel condition.

AQ5

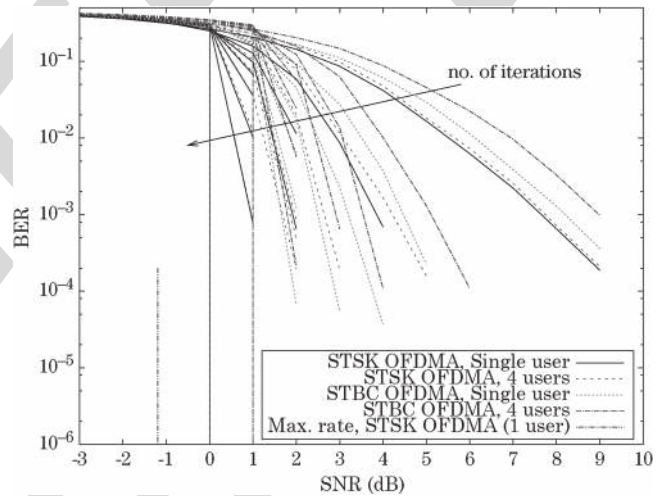


Fig. 4. BER performance of our channel-coded MMSE equalization-based OFDMA STSK (2, 2, 2, 2) that employs BPSK modulation in the dispersive COST207-TU12 channel and the corresponding  $\mathcal{G}_2$ -STBC scheme. The maximum achievable rate for the corresponding scheme for a single user, computed using the EXIT chart's area property, is also shown.

The achievable performance is, however, degraded, when ZF is used 340  
 due to the noise enhancement imposed. The performance of the pro- 341  
 posed STSK-based scheme is also compared to those of the V-BLAST- 342  
 aided [3] and  $\mathcal{G}_2$ -STBC-aided [4], [19] OFDMA/SC-FDMA schemes 343  
 using the same number of transmit and receive AEs ( $M, N$ ) and the 344  
 same throughput per block interval in Fig. 3, which demonstrates the 345  
 efficacy of the proposed scheme. 346

In Figs. 4 and 5, we also characterized the achievable BER perfor- 347  
 mance of the three-stage RSC- and URC-coded OFDMA/SC-FDMA 348  
 STSK (2, 2, 2, 2) binary phase-shift keying (BPSK) scheme that 349  
 relies on interleaved subcarrier allocation strategy in the context of 350  
 the wideband COST207-TU12 channel [11], where we employed 351  
 a half-rate RSC code with a constraint length of  $k_c = 2$  and the 352

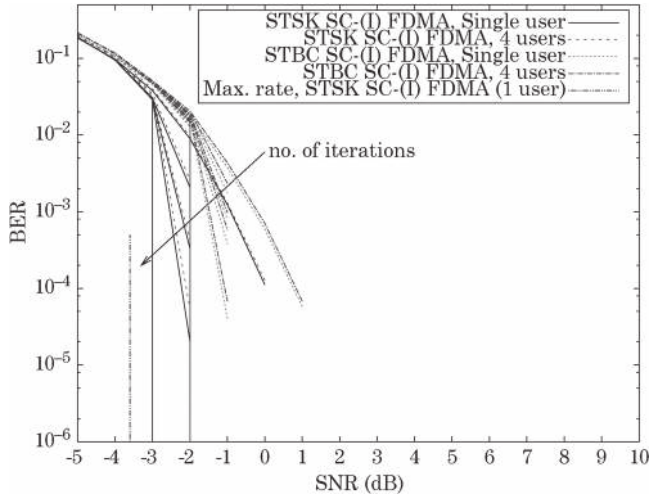


Fig. 5. Achievable BER performance of our channel-coded MMSE-based SC-FDMA STSK (2, 2, 2, 2) with BPSK modulation in the COST207-TU12 channel and the corresponding  $\mathcal{G}_2$ -STBC scheme with similar parameters. The maximum achievable rate of the corresponding scheme with a single user is also shown.

353 octally represented generator polynomials of  $(g_r, g) = (3, 2)_8$ , as  
 354 well as two random interleavers with a memory of 4 608 000 b. The  
 355 numbers of inner and outer decoder iterations were set to  $I_{inner} = 2$   
 356 and  $I_{outer} = 9$ , respectively. We also investigated the performance  
 357 of the SC-LFDMA scheme, and the performance was observed to  
 358 be similar to SC-IFDMA in the coded scenario. (However, the SC-  
 359 LFDMA performance figure has not been included here to limit the  
 360 total number of figures.) The performance of both the OFDMA STSK  
 361 and SC-(I)FDMA STSK has been compared to the corresponding  $\mathcal{G}_2$ -  
 362 STBC benchmarks. The maximum achievable rates of our schemes  
 363 were also calculated by exploiting the so-called area property of  
 364 EXIT charts. To be specific, it was shown in [20]–[22] that the area  
 365 under the inner decoder's EXIT curve at a certain signal-to-noise ratio  
 366 (SNR) quantifies the maximum achievable rate of the system, where an  
 367 infinitesimally low BER may be achieved. The SNRs that correspond  
 368 to the maximum achievable rates of the schemes are also shown in  
 369 Figs. 4 and 5.

370 Fig. 6 portrays the EXIT chart of the SC-FDMA STSK(2, 2, 2,  
 371 4) arrangement combined with QPSK modulation and the IFDMA  
 372 strategy, where the SNR was varied from  $-5$  dB to  $1$  dB in steps of  
 373  $0.5$  dB. It is shown that an open EXIT tunnel is formed at SNR =  
 374  $-4.0$  dB using an interleaver depth of 4 608 000 b. The corresponding  
 375 staircase-shaped decoding trajectory [22] based on bit-by-bit Monte  
 376 Carlo simulations conducted at  $-2.5$  dB is also shown. Thus, it can be  
 377 inferred that an infinitesimally low BER may be achieved at SNR =  
 378  $-2.5$  dB in a UL scenario after  $I_{outer} = 5$  iterations.

## V. CONCLUSION

380 In this paper, an OFDMA/SC-FDMA-aided STSK scheme has been  
 381 proposed, which overcomes the impairments of realistic dispersive  
 382 channels while facilitating multiuser transmissions. The scheme bene-  
 383 fits from the flexible diversity versus multiplexing gain tradeoff offered  
 384 by the recently developed STSK scheme that relies on low-complexity  
 385 single-stream-based ML detection. We quantified the relative merits of  
 386 OFDMA and SC-FDMA when combined with STSK and advocated  
 387 the SC-FDMA-based STSK scheme that relies on the interleaved  
 388 subcarrier allocation in the UL scenario as a benefit of its low PAPR.  
 389 The effects of the spatial correlation between the different AEs of a

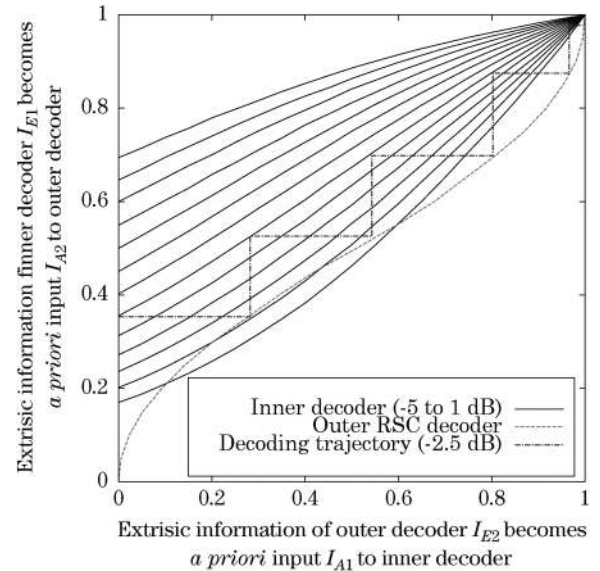


Fig. 6. EXIT trajectory of our three-stage turbo-detected MMSE-based SC-(I)FDMA STSK(2, 2, 2, 4) with QPSK modulation applied in a COST207-TU12 dispersive channel model with  $f_d = 0.01$ . The EXIT trajectory at  $-2.5$  dB is mapped on inner decoder EXIT curves from  $-5$  to  $1$  dB in steps of  $0.5$  dB and the outer RSC decoder EXIT function.

multiple antenna UL, however, have to further be investigated and will  
 be included in our future study.

It is worth mentioning here that the dispersion matrices invoked for  
 constructing our STSK system were optimized by an exhaustive search  
 to minimize the maximum PSEP under the power constraint in (2).  
 However, instead of using an exhaustive search method, a heuristic- or  
 genetic-algorithm-aided optimization of the dispersion matrices [23]–  
 [25] may also be investigated.

The EXIT charts of the proposed scheme converge to the (1.0, 1.0)  
 point of perfect convergence to a vanishingly low BER after a few  
 iterations, thus indicating a sharp decrease of the BER curve.

## REFERENCES

- [1] S. Sugiura, S. Chen, and L. Hanzo, "A universal space-time architecture for multiple-antenna-aided systems," *IEEE Commun. Surveys Tuts.*, vol. 14, no. 2, pp. 401–420, Jan. 2012.
- [2] S. Sugiura, S. Chen, and L. Hanzo, "Coherent and differential space-time shift keying: A dispersion matrix approach," *IEEE Trans. Commun.*, vol. 58, no. 11, pp. 3219–3230, Nov. 2010.
- [3] G. Foschini, G. Golden, R. Valenzuela, and P. Wolniansky, "Simplified processing for high spectral efficiency wireless communication employing multielement arrays," *IEEE J. Sel. Areas Commun.*, vol. 17, no. 11, pp. 1841–1852, Nov. 1999.
- [4] V. Tarokh, H. Jafarkhani, and A. Calderbank, "Space-time block codes from orthogonal designs," *IEEE Trans. Inf. Theory*, vol. 45, no. 5, pp. 1456–1467, Jul. 1999.
- [5] V. Tarokh, N. Seshadri, and A. Calderbank, "Space-time codes for high-data-rate wireless communication: Performance criterion and code construction," *IEEE Trans. Inf. Theory*, vol. 44, no. 2, pp. 744–765, Mar. 1998.
- [6] B. Hassibi and B. M. Hochwald, "High-rate codes that are linear in space and time," *IEEE Trans. Inf. Theory*, vol. 48, no. 7, pp. 1804–1824, Jul. 2002.
- [7] R. W. Heath, Jr. and A. Paulraj, "Linear dispersion codes for MIMO systems based on frame theory," *IEEE Trans. Signal Process.*, vol. 50, no. 10, pp. 2429–2441, Oct. 2002.
- [8] R. Mesleh, H. Haas, S. Sinanovic, C. W. Ahn, and S. Yun, "Spatial modulation," *IEEE Trans. Veh. Technol.*, vol. 57, no. 4, pp. 2228–2241, Jul. 2008.
- [9] J. Jeganathan, A. Ghrayeb, L. Szczecinski, and A. Ceron, "Space shift keying modulation for MIMO channels," *IEEE Trans. Wireless Commun.*, vol. 8, no. 7, pp. 3692–3703, Jul. 2009.

- 431 [10] A. Ghosh, R. Ratasuk, B. Mondal, N. Mangalvedhe, and T. Thomas,  
432 "LTE-Advanced: Next-generation wireless broadband technology," *IEEE*  
433 *Wireless Commun.*, vol. 17, no. 3, pp. 10–22, Jun. 2010.
- 434 [11] M. Patzold, *Mobile Fading Channels*. New York, NY: Wiley, 2003.
- 435 [12] R. Steele and L. Hanzo, *Mobile Radio Communications*, 2nd ed. New  
436 York, NY: Wiley, 1999.
- 437 [13] L. Hanzo, O. Alamri, M. El-Hajjar, and N. Wu, *Near-Capacity Multifunc-*  
438 *tional MIMO Systems (Sphere-Packing, Iterative Detection and Coopera-*  
439 *tion)*. New York: Wiley, May 2009.
- 440 [14] H. G. Myung, J. Lim, and D. J. Goodman, "Single-carrier FDMA for  
441 uplink wireless transmission," *IEEE Veh. Technol. Mag.*, vol. 1, no. 3,  
442 pp. 30–38, Sep. 2006.
- 443 [15] L. L. Yang, *Multicarrier Communications*. Chichester, U.K.: Wiley,  
444 Jan. 2009.
- 445 [16] A. Wilzeck, Q. Cai, M. Schiewer, and T. Kaiser, "Effect of multiple-carrier  
446 frequency offsets in MIMO SC-FDMA systems," in *Proc. Int. ITG/IEEE*  
447 *Workshop Smart Antennas*, Vienna, Austria, Feb. 2007.
- 448 [17] L. Hanzo, M. Munster, B. J. Choi, and T. Keller, *OFDM and MC-CDMA*  
449 *for Broadcasting Multiuser Communications, WLANs and Broadcasting*.  
450 New York: Wiley, Jul. 2003.
- 451 [18] J. R. Barry, E. A. Lee, and D. G. Messerschmitt, *Digital Communication*,  
452 3rd ed. Berlin, Germany: Springer-Verlag, 2003.
- [19] S. Alamouti, "A simple transmit diversity technique for wireless commu- 453  
nications," *IEEE J. Sel. Areas Commun.*, vol. 16, no. 8, pp. 1451–1458, 454  
Oct. 1998. 455
- [20] M. Tuchler, "Design of serially concatenated systems depending on the 456  
block length," *IEEE Trans. Commun.*, vol. 52, no. 2, pp. 209–218, 457  
Feb. 2004. 458
- [21] J. Hagenauer, "The EXIT chart—Introduction to extrinsic information 459  
transfer in iterative processing," in *Proc. Eur. Signal Process. Conf.*, 460  
Vienna, Austria, Sep. 2004, pp. 1541–1548. 461
- [22] S. Ten Brink, "Convergence behavior of iteratively decoded parallel con- 462  
catenated codes," *IEEE Trans. Commun.*, vol. 49, no. 10, pp. 1727–1737, 463  
Oct. 2001. 464
- [23] F. Babich, A. Crismani, M. Driusso, and L. Hanzo, "Design criteria 465  
and genetic algorithm aided optimization of three-stage concatenated 466  
space–time shift keying systems," *IEEE Signal Process. Lett.*, vol. 19, 467  
no. 8, pp. 543–546, Aug. 2012. 468
- [24] M. Jiang and L. Hanzo, "Unitary linear dispersion code design and opti- 469  
mization for MIMO communication systems," *IEEE Signal Process. Lett.*, 470  
vol. 17, no. 5, pp. 497–500, May 2010. 471
- [25] R. Rajashekar, K. Hari, and L. Hanzo, "Field-extension-code-based dis- 472  
persion matrices for coherently detected space–time shift keying," in 473  
*Proc. IEEE GLOBECOM*, Dec. 2011, pp. 1–5. 474

IEEE  
PROOF



## AUTHOR QUERIES

AUTHOR PLEASE ANSWER ALL QUERIES

AQ1 = Please provide keywords.

AQ2 = Acronyms that were mentioned only once should be spelled out, hence the omission of STTC, LDC, and SM. Please check if this is correct.

AQ3 = Editing was made to avoid confusion in hyphenations. Please check if this did not change the sentence's intended meaning.

AQ4 = Please check if the editing made did not change the sentence's intended meaning. Otherwise, provide the missing term or phrase.

AQ5 = Please check if the editing made (especially the use of serial comma) did not change the sentence's intended meaning. Otherwise, provide the missing term or phrase.

END OF ALL QUERIES

IEEE  
PROOF